Title

Stiffness Variable Polymers Comprising Phase-Changing Side-Chains: Material Syntheses and Application Explorations

Journal

Advanced Materials, 34(21)

ISSN

0935-9648

Authors

Gao, Meng
Meng, Yuan
Shen, Claire
et al.

Publication Date

2022-05-01

DOI

10.1002/adma.202109798

Peer reviewed

WILEY-VCH

DOI: 10.1002/((please add manuscript number))
Article type: Review

Stiffness variable polymers comprising phase-changing side-chains: material syntheses and application explorations

Meng Gao, Yuan Meng,* Claire Shen, and Qibing Pei*

Dr. M. Gao, Dr. Y. Meng, C. Shen and Prof. Q. Pei
Soft Materials Research Laboratory, Department of Materials Science and Engineering, Henry Samueli School of Engineering and Applied Science, University of California, Los Angeles, CA 90095, USA
*Corresponding author. E-mail: ymeng5@g.ucla.edu, qpei@seas.ucla.edu

Dr. M. Gao
College of Light Industry Science and Engineering, Tianjin University of Science and Technology, Tianjin 300457, China

Keywords: Stiffness variable polymer, phase transition, side-chain crystalline, bottlebrush, alkyl chain, shape memory, dielectric actuator

Stiffness variable materials have been applied in a variety of engineering fields that require adaptation, automatic modulation, and morphing because of their unique property to switch between a rigid, load-bearing state and a soft, compliant state. Stiffness variable polymers comprising phase-changing side-chains (s-SVPs) have densely grafted, highly crystallizable long alkyl side-chains in a crosslinked network. Such a bottlebrush network-like structure gives rise to rigidity modulation as a result of the reversible crystallization and melting of the side chains. The corresponding modulus changes can be more than 1000 fold within a narrow temperature span, from ~10^2 MPa to ~10^2 kPa or lower. Other important properties of the s-SVP, such as stretchability, optical transmittance, and adhesion, can also be altered. This work reviews the underlying molecular mechanisms in the s-SVP's, discusses the material's structure-property relationship, and summarizes important applications explored so far, including reversible shape transformation, bistable electromechanical transduction, optical modulation, and reversible adhesion.

1. Introduction

Synthetic materials are usually designed with a certain stiffness to satisfy the operational requirements and economic constraints of specific applications. For example, carbon nanotube-reinforced polymer composites have a Young's modulus as high as 500 GPa for applications demanding high-strength,[1] whereas elastomers for epidermal interfaces have a desired modulus on the order of 10^1 kPa.[2] Most of these synthetic materials have a constant modulus that does not change significantly during the course of operation, providing high stability. Consequently, they lack the adaptability biological muscles have for variable working environments. Emerging opportunities in airborne and submarine vehicles, agricultural manipulations, biomedical devices, and wearable electronics require materials with variable rigidity to respond to dynamically changing conditions.[3-6] The mechanical impedance of such materials can be altered or fine-tuned to allow the system to adapt without a sophisticated control algorithm. For example, when grasping a fragile object such as an egg using a gripper, a stiffness variable material provides an adaptive contact force to optimally complete the task. Similarly, bio-inspired robots and wearable exoskeletons require stiffness variable materials capable of a large stiffness change to provide structural load-bearing and mechanical work output. In the softened state, the material can deform to locomote, maneuver, and absorb the energy arising from a collision or when interfacing with the human body. Some applications, such as medical endoscope designs, involve "move-and-hold" operations. This is where a variable-stiffness structure that holds a particular orientation in space or rigidly supports a load is able to become deformable on demand to change shape or reposition.[7] Other potential applications that can benefit from variable stiffness materials include biomechanically compatible sensor insertions for neural implants, vibration and noise control in aerospace structures, and conformal shape morphing robotic systems.

1.1 Requirements of Stiffness Variable Materials

To impart the perceived smart and adaptive systems with versatile and advantageous functionalities matching or surpassing those of natural systems, the stiffness variable materials should possess the following important features:

(1) Wide modulus variation: A range of modulus variation greater than 100 or even 1000-fold is required. A high modulus is desired for load-bearing and supporting freestanding structures, while a low modulus provides conformation, shape transformation, energy absorption, and dissipation.

(2) Mild stimulus: A mild stimulus to trigger the stiffness variable operation, such as a narrow temperature span in thermally triggered materials, is essential to maintaining desired functions in a broad temperature range with rapid and low energy consumption upon transition.

(3) Accessible modulation control: The external trigger for modulation is accessible and easy to control.

(4) Reversible stiffness change: The reversible stiffness change property is required in applications with multiple operation cycles.

(5) Fast stiffness change: A rapid stiffness change is crucial for dynamic operations that demand a short response time.

(6) Solid state: It is preferable that the material and the stiffness changing operation process do not involve any liquids or liquid state. Otherwise, hermetic encapsulation or special packaging would be required, which adds additional costs and constraints.

(7) Cost-effective process: The material should be easy to process for mass production and broad deployment. Being compatible with 3D printing is quite desirable to readily fabricate complex devices structures.

1.2 Natural and Synthetic Stiffness Variable Materials

Nature has long been a source of biological materials with variable stiffness that inspire researchers to create artificial ones with similar or even superior properties. A great example is the sea cucumber *Cucumaria frondosa* that can reversibly regulate its tissue modulus through cross-linking interactions among adjacent collagen fibrils, significantly affecting the strength of the viscoelastic matrix inside the multiphase dermis.[8, 9] Stiffness variation can also be found in plants where diffusion of water for swelling and shrinking are responsible for the mechanical change.[10] A more familiar example of natural variable stiffness material is the human skeletal muscle, which can adjust its rigidity via sliding of thin filaments over thick filaments in muscle sarcomeres. This results in controllable and adaptive force output for various body motions.[11, 12] These strategies have inspired the design of new variable stiffness materials.

Variable rigidity has been obtained in many synthetic materials, including metals, polymers, magnetic fluid, *etc*. Shape memory alloys like nickel-titanium alloys can transition between two shapes, each with its distinctive crystalline structure, when subjected to temperature or magnetic stimulus.[13] Shape memory alloys provide an adequate rigid state for work output with an elastic moduli on the order of 10^2–10^4 MPa. Their soft state is normally 3-4 times softer than the stiffened structure,[14] which is still overly stiff for living organisms (for example, skin or

muscle tissue) with moduli on the order of 10^1–10^5 kPa.[4] Alternatively, low-melting-point alloys (LMPAs), such as liquid metal eutectic gallium indium (EGaIn), change from liquid to solid reversibly at the melting temperature, with an exceptionally large ratio of modulus change up to 10^4.[15] Likewise, magneto-rheological fluids (MRFs) respond instantly to varying levels of a magnetic field, changing from a free-flowing liquid to a semi-solid due to the increased apparent viscosity under magnetic strength.[16] Like LMPAs, the liquid state of the MRFs limits these materials' applications unless proper encapsulation is implemented.

Stiffness variable polymers (SVPs), including shape memory polymers (SMPs) and liquid crystal elastomers (LCEs), exhibit dynamic mechanical behaviors in response to environmental triggers such as temperature, light, moisture, pH, and magnetic field. The underlying driving force can be reversible crosslinking, dynamic bonding, or phase transformation. Among them, temperature-stimulated SVPs based on crystalline-amorphous phase transition feature large and reversible strain capability at the amorphous state, easy access of thermal activation, being solid-state, and compact. An elevated temperature of the SVPs can produce a modulus change up to a few hundred or thousand fold.[17]

1.3 Advantageous Features of S-SVPs

The phase-changing moieties of the SVPs could be either in the polymer main chain or side groups. While the main-chain crystallizable SVPs have been quite widely studied,[18-20] the SVPs comprising phase-changing side-chains (s-SVPs) have not received due tractions, but can have important advantages. Grafted at high density, the s-SVPs with bottlebrush-like long alkyl side chains provide higher mobility than main-chain segments to afford relatively fast crystallization, high crystallinity, and fast relaxation. This gives rise to a sharp phase change within a narrow temperature span, enabling a transition from a rigid (modulus ~ 10^2 MPa), crystalline plastic to a super-soft (modulus ~ $10^{1\text{-}2}$ kPa) rubbery material. An s-SVP can assume specific robust shapes under load-bearing working conditions and can be programmed into different configurations via thermal stimulation. The narrow temperature span to complete the transition helps minimize energy expenditure, transition time, and thermal damage to neighboring components. These features are well suited for applications in wearable electronics, bio-inspired robotics, and implantable devices.

The recent developments of s-SVPs in material synthesis, important properties accompanying the reversible phase change, and corresponding applications are reviewed and summarized in **Figure** 1. The molecular origins of the s-SVP's narrow transition temperature span and large modulus variation will be discussed in Section 2. Commonly used s-SVP and

corresponding copolymer and composite systems will be introduced in Section 3, with an emphasis on the modulation of the transition temperature and modulus change. Section 4 discusses reversible shape transformation applications based on the large modulus change, bistable electro-mechanical transduction, optical modulation for smart windows, and reversible adhesion. The bulk polymerization to form the s-SVP allows for the addition of functional fillers such as hydrogels and photonic crystals in the SVP matrix, greatly broadening the scope of applications.

2. Polymers Exhibiting Large Variable Stiffness

The origin of large modulus modulation in stiffness variable polymers can be explained by the theory of rubber elasticity. The tensile modulus E of an ideal elastomer under strain is determined by:[21]

$$E=3\rho RT/(\bar{M}_c) \quad (1)$$

where ρ is the density of the elastomer, R is the gas constant, T is the absolute temperature, and $\bar{M}_c$ is the number-average molecular weight of the chain segments between consecutive crosslinks. $\bar{M}_c$ is related to the polymer chain between the adjacent temporary entanglement points and characterizes both the physical and chemical crosslinks in the elastomer network. The modulus reflects the elastomer's molecular architecture and is inversely proportional to $\bar{M}_c$. Therefore, the stiffness of the polymer can be adjusted through switchable netpoints, which connect the switchable segment dynamically. Based on the triggering mechanism and molecular structure, stiffness variable polymers can be categorized into two categories: molecular switch-based SVP and phase transition-based SVP, as shown in **Figure** 2.

Molecular switch-based SVP utilizes chemically reversible covalent bonds or physical supramolecular interactions as the netpoints to vary the average molecular weight of chain segments between crosslinks to adjust polymer stiffness. The stiffness change in SVP with reversible covalent bonds is accomplished by stimuli-controllable coupling and decoupling of dynamic covalent linkages such as Diels-Alder reaction,[22-24] oxidation/redox reaction of the mercapto group,[25] phenylboronic acid–diol interactions,[26] and Schiff base linkages.[27] For SVP based on supramolecular interactions, reversible stiffness change processes occur through dynamic dissociation and recombination of non-covalent interactions such as hydrogen bonding,[9, 28, 29] host-guest interactions,[30] and metal-ligand coordination.[31-33] In these cases, functional groups have to be introduced into the given polymer matrix, which allows stimuli-controlled formation of reversible switches during the stiffness modulation process.

Phase transition-based SVP typically consists of phase-changing polymer chains, either in

the main chain or the side chain, with varying chain mobility under temperature stimulus. Phase changing is an entropic phenomenon that is associated with the relaxation behavior of the polymer chains or segments.[34, 35] Typically, SVP consists of switching segments that are capable of reversible phase transformation (crystallization/ melting transition, glass/ rubbery transition, and anisotropic/ isotropic transition) at a specific range of temperatures.[36-38] Liquid crystal polymers that depend on alignment directions and anisotropic/ isotropic phase transitions (nematic, cholesteric, smectic, or isotropic) [39] will not be discussed here. For SVP based on melting and glass transition, the polymer structure is rigid with limited molecular motion below the phase changing temperature. When heated above the transition temperature, polymer chains become mobile and large-scale molecular motion becomes possible.[18] The polymer undergoes volume and density change at the transition point, which inevitably leads to stiffness tuning behavior. The volume change at melting is a first-order thermodynamic transition that is abrupt and discontinuous, providing large chain mobility in the soft state and a large stiffness change. On the other hand, glass transition is a kinetic phenomenon[40] that demonstrates decreased stiffness modulation performance with smaller and continuous volume changes.

Currently, phase transition-based SVP is the most advantageous and investigated because of its relatively simple synthetic chemistry.[41] For SVP based on main-chain phase-change (m-SVP), the crystallizable segments are crosslinked in the polymer backbone, whereas s-SVPs have a bottlebrush network with crystallizable moieties dangling along the backbone. The phase-changing side-chains will have uniform molecular lengths unaffected by crosslinking, which demonstrates fewer molecular mobility restrictions. This unique crosslinked bottlebrush network structure of s-SVP results in a sharp phase change, enabling a transition from rigid, crystalline plastic to a super-soft, deformable rubber material within a narrow melting temperature range. The detailed mechanism and properties of s-SVPs are further detailed in the following section.

3. Side-chain Crystallizable SVP

3.1. Mechanism of Large Modulus Change

The unique s-SVP network structure with densely grafted, highly crystallizable side chains gives rise to a sharp phase change, enabling large modulus transition from a rigid (modulus ~10^2 MPa), crystalline plastic to a super-soft (modulus ~10^{1-2} kPa), deformable rubber material, separated by a narrow melting temperature span. The reversible phase change

of the crystallizable side chains in s-SVPs and its impact on the polymer's modulus modulation and transition temperature span are discussed both under the melt state and the crystalline state.

3.1.1. S-SVP in the Melt State

A graft polymer has one or more species of polymer blocks connected to the backbone as side chains. In the melt state of a crosslinked graft polymer, side chains with a degree of polymerization n_{sc} and bond spacing n_g play the role of a solvent that dilutes effective elastic chain (backbone) density. Here, bond spacing represents backbone bonds between graft points. The degree of backbone dilution is described by a composition parameter, which corresponds to the molar fraction of polymer backbones in a graft polymer:

$$\varphi = \frac{n_g}{n_g + n_{sc}} \qquad (2)$$

In the melt of a graft polymer with identical flexible side chains and chain segments in the backbones, Dobrynin *et al.* introduced the crowding parameter Φ:

$$\Phi \approx \frac{v}{(lb)^{3/2}} \frac{\varphi^{-1}}{n_{sc}^{1/2}} \qquad (3)$$

where v is the monomer excluded volume, l is the monomer projection length, and b is the Kuhn length.[42-44] The crowding parameter describes the degree of mutual interpenetration between neighboring macromolecules in a graft polymer melt. With increasing side chain crowdedness, graft polymers can be categorized into comb polymer and bottlebrush polymer. For comb polymers with $\Phi < 1$, neighboring graft polymers interpenetrate. Similar to regular linear coiled chains, most side chains and backbones maintain their unperturbed ideal chain conformations. The backbones remain flexible with a Kuhn length equal to that of linear chains. On the other hand, in bottlebrush polymers with $\Phi > 1$, steric repulsion of densely grafted polymers behaves as a whole like a semiflexible rod with negligible overlap and markedly lower backbone chain entanglement (**Figure** 3).[42, 44]

S-SVP with crystallizable side chains dangle on the backbone is densely grafted bottle brush polymer. The unique bottlebrush molecular architecture effectively gives rise to ultra-soft polymer networks.[45-48] Network modulus is inversely related to the average relative molecular mass between crosslinks (Equation 1). Inside a crosslinked bottlebrush network, diluted elastic backbones account for only a small portion of the overall network mass. This results in a largely expanded $\overline{M}_c$ and a much lower modulus compared to linear chain networks with the same number-average DP of backbone strand n_x. In general, chain entanglements are inherent to conventional linear networks and inhibit the network modulus to be lower than $E_e = 10^2 \sim 10^3$ kPa.[45, 49] In a bottlebrush network, backbone extension is followed by extension of side chains

with increasing grafting density, so crosslinked backbones cannot maintain their ideal coiled conformation (Figure 3a). This causes intrinsic chain entanglements to be eliminated, resulting in a network modulus that is further lowered well below linear network limits. This produces s-SVP, a bottlebrush network with an ultra-low modulus of 30 kPa and significantly high strain at a break of 1200%.[50] In fact, by carefully tuning the architectural parameters such as n_{sc}, n_g, and n_x, it is possible to replicate mechanical properties from super-soft to super-firm materials.[51]

3.1.2. S-SVP in the Crystalline State

The bottlebrush s-SVP densely grafted with crystallizable, long alkyl chains imparts high crystallinity and a sharp rigid-to-rubbery transition.[52, 53] The crystallization of the long alkyl side chains, such as stearyl, [54-57] takes place at a fairly sharp melting point. It is distinct from not only the second-order transition phenomenon exhibited by the lower acrylates (a minimum requirement of carbon atoms to form side chain crystallites is 9), [58] but also the usual type of linear polymer crystallization (alignment of the polymer chain itself).[59] Below the melting temperature, the long alkyl chains adopt a crystalline aggregate structure that renders the s-SVP material additional mechanical robustness. Above this temperature, the packing of the side chains is amorphous and the crosslinked bottlebrush network becomes extremely soft and flexible.[53]

In the s-SVP bottlebrush network, both side chains and backbones adopt stretched configurations, which are prone to packing and forming densely stacked crystallite with ordered structures. In particular, as suggested by Plate and Shibaev, *et al*., the alkyl side chains in poly(n-alkyl acrylates) form inverse combs in the planar side-chain structure, while the layered polymer backbones remain extended and stack to give a 3D layer-by-layer ordered structure, as shown in Figure 3b.[60, 61] This packed side-chain crystallite structure is strikingly different from the chain-folded crystallite lamella commonly found in linear semi-crystalline polymers.[62, 63] Chain segments on the backbone of the linear semi-crystalline polymers are involved in the crystallization, and the backbone crystallization is a rather complicated process, which can be impacted by the presence of crosslink points, local entanglements, and chain length polydispersity. These lead to a wide distribution of crystallite size and a large melting temperature span. In the s-SVPs, the dangling side chains have high mobility, little entanglement, and a uniform length. Thus, the crystallization of these side chains leads to a narrow distribution of crystallite size. The s-SVPs demonstrate a narrow phase transition temperature span. It is interesting that the narrow melting range of the side chain crystallite is

found to be independent of cooling temperature.[64] The specific melting point of the bottlebrush polymer can be conveniently modulated within a broad range by tuning the amount of side chain monomer in the s-SVP formulation.[52]

For bottlebrush polymer S-SVP with alkyl side chain, there exist two glass transition temperatures (T_g): one from the backbone and one from the side groups. In poly(n-alkyl methacrylate) (4≤C≤12) system, the backbone T_g depends primarily on the backbone chain flexibility and the side group bulkiness (occupied volume).[65] Besides that, a polyethylene(PE)-like glass transition (α_{PE}) of alkyl side chain is observed at lower temperatures.[66] As indicated by Briner *et al.*, the α_{PE} process is originated from self-assembled confinements of alkyl nanodomains.[67] Similar to the nanometer confinement behavior of glass-forming liquids constrained in nanoporous mold,[68-70] solid N-alkylated polymers also exhibit cooperative dynamic changes when the confinement size of alkyl chain domains becomes comparable to the size of cooperatively rearranging regions as a characteristic length scale of the dynamic glass transition in the amorphous bulk material, leading to the deviation of dynamic glass transition from the behavior in the bulk. The alkyl nanodomain size and the glass transition temperature of α_{PE} process $T_g(\alpha_{PE})$ are mainly determined by the number of alkyl carbon atoms per side chain, and depend slightly on the microstructure of the main chain. $T_g(\alpha_{PE})$ declines with decreasing size of the alkyl nanodomains. The coexistence of two glass transitions takes place in other side-chain polymers with long alkyl groups, such as poly(di-n-alkyl itaconates)[71] and 'hairy rod' polyimides.[72] For poly(di-n-alkyl itaconates) (7≤C≤11), the transition occurring at the lower temperature originates in the side groups and is a result of the independent cooperative relaxation of the alkyl side chains, while that observed at higher temperatures reflects the glass-rubber transition of the main chain backbone and the cooperative motion of the entire molecule.[71] The relaxation temperatures for the α_{PE} process in these series are similar to those in the poly(n-alkyl acrylates) and poly(n-alkyl methacrylates) series.

The dynamic behavior near the glass transition is critical as the drastic changes in physical properties of polymeric materials, concomitant of the transition from rubbery to glassy states upon cooling, determine their mechanical properties. The material property of fragility, quantifying the steepness of the temperature dependence of the segmental relaxation time close to T_g, categorizes glass-forming materials into"fragile" and "strong" systems.[73] Generally speaking, polymers with rigid backbones exhibit higher fragility than those with flexible backbones.[65] The fragility of α_{PE} process rises with increasing side chain length and alkyl nanodomain size, indicating a shift towards a polyethylene-like glass transition.[67] Both poly(n-

alkyl acrylate) and poly(n-alkyl methacrylate) series show a strong-to-fragile transition for the α_{PE} process with increasing side chain length.

3.2. Material Selection for s-SVP

For s-SVP, the side chain needs to be able to form packed semicrystalline lamellae below the transition temperature and turn amorphous when heated. Whether the polymer can crystallize or not depends on its molecular structure. The presence of straight chains with regularly spaced side groups facilitates crystallization, which means side chains with a high degree of stereoregularity typically possess a high crystallinity index and phase changing performance. To fabricate s-SVP, several side chains, including the alkyl chains, perfluoroalkyl chains, and ethylene oxide (EO) side chains, have been investigated. Table 1 summarizes the representative s-SVPs, their structures, transition temperatures and span, and modulus variation range.

Alkyl chain-based s-SVP, such as poly(n-alkyl acrylate)s[74] and poly(n-alkyl methacrylate)s,[75] are most commonly used as the building block for phase-changing material, with CH_2 units exhibiting perfect stereoregularity. For poly(n-alkyl acrylate)s and poly(n-alkyl methacrylate)s, they can be synthesized by simply photo-polymerizing the corresponding monomer, making the fabricating method efficient and cost-effective. Other n-alkylated polymers with different backbones can be synthesized by linking the alkyl chain onto the main chain with various chemical junctions. Several examples of N-alkylation methods are introduced here to show how these s-SVP materials are fabricated. By UV grafting octadecanethiol onto alkyl-based epoxy resin via thiol-ene click chemistry, epoxy-based s-SVP are easily prepared.[76] Alkylated poly(vinyl chloride) (PVC) polymers are prepared through a nucleophilic substitution reaction between PVC and n-alkyl mercaptan, where the S atom acts as the chemical junction between PVC backbone and alkyl side chain.[77] Octadecylated poly(vinyl alcohol) (PVA) s-SVP polymer is normally achieved by grafting bromooctadecane onto PVA via the alkylation method.[78] N-alkylation reactions between a pyrrole monomer and n-alkyl bromide are used to fabricate N-alkylated polypyrrole.[79] These reactions provide feasible approaches to grafting alkyl chains onto different backbones and exhibiting s-SVP performance for different applications. Apart from alkyl-substituted polymers, polymers with relatively hydrophilic ethylene oxide units[80-82] and hydrophobic perfluoroalkyl chain[83-87] as side chains also exhibit phase changing behavior. The specific wettability of these s-SVP results in unique properties. For example, polymers containing perfluoroalkyl side chains demonstrate outstanding antiadhesive and oil-repellent properties due to the enrichment of fluorine moieties

at surface layers, making them suitable for microelectronic, antifouling, and medical applications.

Since s-SVP are composed of the backbone and side-chain, they are able to self-assemble into various ordered structures and demonstrate characteristic crystallization behaviors in the crystalline state. In general, the packing mode and the crystallization ability of s-SVP largely depend on the rigidity of the backbone and the length of the pendent side chains.[88] When the polymer backbone is rigid, crystallization requires a longer side chain because the section of the side chain closest to the backbone is unable to crystallize and remains amorphous. In regions far from the polymer backbone, the side chains become flexible to overcome the constraints imposed by the relatively stiff polymer backbone and are able to crystallize.[89] In other words, for s-SVP with a rigid backbone, the ordered state of side chains participating in the crystallites is lower because of the decreased side-chain conformational adjustment ability. Conversely, a flexible backbone allows more side chains, such as methylene groups, to enter the crystal lattice and form crystallites. To realize side-chain crystallization for a flexible polymer skeleton such as polyethylenimine,[90] six carbon atoms per side chain are required, whereas a rigid polymer skeleton such as poly(p-benzamide),[91] polypyrrole,[79] and polyaniline[92] requires ten or more carbon atoms. Similarly, by comparing the side group crystallization ability of poly(n-alkyl acrylate)s and poly(n-alkyl methacrylate)s, the minimal length of an alkyl side chain for side-chain crystallization is dependent on polymer backbone flexibility.[93] The polymer backbone is more rigid for methacrylates than for acrylates, reflecting the additional steric hindrance from the extra methyl group. For poly(n-alkyl acrylates), an alkyl chain with nine carbon atoms is the minimal side chain length for crystallization.[88, 94] Similarly, for poly(n-alkyl methacrylates), at least twelve carbon atoms are required to form side-chain crystallites. This effect applies not only to N-alkylated s-SVP, but also to fluorinated n-alkyl acrylate and methacrylate polymers that can easily crystallize into a crystal lattice when the backbone is a flexible main chain.[95] The rigidity of polymer backbone also plays an important role for the transition temperature span. S-SVP with soft backbones would have a narrow melting peak. For example, alkylated polyethylenimine demonstrates a more sharp transition peak compared with the broad one of alkylated poly(p-benzamide).[91] This trend is consistent with the transition temperature span of different s-SVPs shown in Table 1.

The length of side chains also affects the transition temperature as shown in **Figure 4**a. The melting temperature, freezing temperature, and enthalpy increases with increasing side-chain length. [77, 79, 96] Using alkylated poly(vinyl chloride) shown in Figure 4b as an example, when the side chain carbon atom increases from n = 12 to 18, both the melting temperature (T_m) and

crystallization temperature (T_c) increase linearly. T_m increases from 36.0 to 66.3 °C, T_c changes from 18.4 to 48.5 °C, and the change of enthalpy ΔH_m changes from 64 to 166 J/g.[77] The increased alkyl side-chain carbon atoms promote more CH_2 groups to participate in the formation of side-chain crystallites. This phenomenon also applies to other side-chains, such as the perfluoroalkyl chain.[85]

3.3. S-SVP Copolymers and Composites

By introducing a second or third component into s-SVP, the transition temperature and modulus change may be tuned.

3.3.1 Transition Temperature of S-SVP Copolymers and Composites

When mixing two s-SVP with different alkyl side-chain lengths, the resulting co-polymers exhibits a T_m ranging in between the two homopolymers. As shown in Figure 4c, the transition temperature of stearyl acrylate (SA) and tetradecyl acrylate (TA) copolymer can be tuned within the range of 25-48°C by adjusting the ratio of the co-monomers.[50] Meanwhile, the narrow transition temperature span is maintained. Other alkyl chains, such as hexadecyl and dodecyl, can also effectively alter the transition temperature.

Other monomers and network-forming oligomers may also be incorporated into the system to modify important properties such as high elasticity and toughness. We synthesized a series of s-SVPs using SA as the phase-changing moiety, a urethane diacrylate (UDA) comprising long polyether diol segments to form the polymer matrix, and trimethylolpropane triacrylate (TMPTA) to raise the crosslink density. The weight ratio of SA:UDA determines the phase change temperature from ~ 45°C at an 80:20 ratio to 35 °C at a 50:50 ratio as illustrated in Figure 4d. With increasing UDA and TMPTA, the transition temperature span is broadened, likely due to limited mobility of the alkyl chains and a broader size distribution of the crystallites. This is quite different from the copolymers of alkyl acrylates with different alkyl chain lengths, which maintain a relatively narrow transition temperature span while the transition temperature is modified.

When a pre-polymerized elastomer, such as polybutadiene[97] and butyl rubber,[98] is added in the s-SVP matrix, the melting and recrystallization temperatures of the alkyl chain domain are independent of the rubber content, as a result of clear phase separation between the elastomer matrix and the newly-formed S-SVP domain. By a similar principle, when paraffin, a phase-changing compound, is added to an allyl-based epoxy resin, an s-SVP, the resulting blend exhibited both the transition temperatures of the s-SVP matrix (35.9 °C) and pristine

paraffin (59.0 °C).[99] Varying the weight ratio of the two ingredients did not significantly alter the melting temperature of the blends, as shown in Figure 4e. Furthermore, by adding long-chain normal alkanes with different chain lengths into poly(stearyl methacrylate) matrix, multiple individual melting peaks were observed (Figure 4f).[100]

3.3.2 Modulus of S-SVP Copolymers and Composites

The modulus change can also be adjusted by adding a second component. Copolymerizing s-SVP with different side-chain lengths does not significantly change the modulus, especially when the alkyl chain lengths are not very different. For example, when adding hexadecyl acrylate (HA) into SA at different ratios, the resulting copolymers' storage moduli during the rigid-to-rubbery transition remain largely unchanged; the rigid-to-soft modulus variation is around 5000 for the HA: SA ratios from 7:1 to 1:7, while the transition temperature is increased from 33 to 43 °C (**Figure 5**a).[101] Copolymerization with a co-monomer of very different nature would substantially modify the modulus modulation. For instance, by introducing UDA, which cures to form a soft elastomer with large elongation, the storage moduli of the SA-UDA copolymers in both rigid and rubbery states are modified dependent on the SA: UDA ratio (Figure 5b).[52] In the rigid state, a lower SA: UDA ratio leads to decreased percentage of crystallinity and thus a smaller modulus. In the rubbery state, lower SA: UDA ratios result in a higher fraction of the cross-linkable UDA moieties. This leads to higher cross-link density and therefore higher storage modulus. Thus, the change of storage modulus during the rigid-to-rubbery transition of the SA−UDA copolymers attenuates from 1066-fold to only 15-fold when the SA fraction is reduced from 80% to 40%. Other elastic materials, such as synthetic rubbers[97, 98] and hydrogels,[102, 103] are also utilized as additives to increase the strain capacity and recovery performance of the s-SVP.

Adding a rigid component could also directly tune the modulus variation. We used bacterial cellulose (BC) nanofibers to form a percolative network within the s-SVP matrix, increasing the storage modulus from 300 MPa for a neat s-SVP matrix, to as high as 1 GPa for the BC-s-SVP nanofiber composite.[101] This composite is dual responsive to temperature, which softens the s-SVP network, and water, which softens the BC nanofibers (Figure 5c). When both networks are softened, the modulus of the composite is reduced to 40 kPa, leading to a 24,000 fold of modulus modulation in the BC-s-SVP composite. This large modulus modulation is reversible and can be repeated.

Reversible bonds incorporated in s-SVP allow for further modulus variation. We found that adding a small amount of acrylic acid (AA) helps to increase the modulus change,

mechanical toughness, and tensile strain (Figure 5d).[104] The hydrogen bonding from the carboxylic acid group in AA contributes to the modulus both at room temperature and elevated temperature. At room temperature, the carboxylic acid groups form double hydrogen bonding dimers to increase the stiffness. Increasing the temperature weakens hydrogen bonding and diminishes its stiffening effect, but the reversible bond breaking and formation enhances the toughness of the elastomer. Other stimulus-responsive reversible bonds have also been explored.[105] Taking metal-ligand interaction as an example, the tridentate Fe(III)–carboxylate coordination introduced to the stearyl methacrylate (SMA) system can effectively reconfigure the network structures and adjust the mechanical strength (Figure 5e). If stepwise modulus switching is desired, one may utilize the s-SVP mentioned above containing long-chain normal alkanes.[100] This system avoids the eutectic crystallization of phase transition components and allows for multiple independent modulus variations (Figure 5f).

4. Applications

The reversible phase transformation of the s-SVP could be utilized to design a number of different applications. First of all, an s-SVP may be used as SMPs. Unlike typical SMPs, the shape transformation of the s-SVPs could be implemented in a narrow temperature span. The polymer at the softened state may be actuated like a dielectric elastomer, leading to bistable electro-mechanical transduction. The large change of refractive index during the phase change can be exploited to modulate optical transmission. The ultralow modulus at elevated temperatures is useful to obtain reversible adhesion. These applications are described in the following four sections.

4.1. Reversible Shape Transformation

4.1.1 Mechanism of Reversible Shape Transformation

Materials that can be transformed from one shape to another upon appropriate external stimuli (**Figure 6**a) are useful for diverse applications in aerospace engineering, biomedical devices, flexible electronics, and soft robotics.[41, 106-111] The reversible modulus change of the s-SVPs derived from the crystalline-amorphous transition of the side-chains is different from that in conventional SMP due to the high crystallinity of the long alkyl chains at ambient temperatures and their high mobility at an elevated temperature.[53] The main chains are crosslinked, which allow the network to elastically deform and return to its original shape once the external load is removed at the amorphous state. Figure 6b illustrates the phase changing and shape programming/memory processes. The original s-SVP in its crystalline and permanent

shape is heated up to the amorphous state when it is deformed under external stress. The deformed structure is fixed at its desired temporary shape after cooling down when the re-crystallized side chains stiffen the matrix. The crystalline structure blocks movement of polymer molecular chains. The permanent shape can be restored by heating the polymer above its transition temperature, where the entropic elasticity of the polymer chain will help to recover its original geometry. The 3D stress-strain-temperature curve of an SA-UDA copolymer s-SVP shown in Figure 6c depicts a typical shape memory cycle. The robust phase transformation and relatively high crosslinking density of s-SVP result in a nearly 100% shape fixity ratio (R_f) and shape recovery ratio (R_r).[52, 104, 112]

4.1.2 Materials for Reversible Shape Transformation

Su *et al*. used butyl rubber (BR) as the matrix builder for SA to enhance the toughness and stretchability (**Figure 7**a).[98] Interestingly, the composite exhibited a significantly higher toughness than the individual components. Similarly, polybutadiene rubber was also used to interconnect stearyl acrylate, achieving high fixity (>90%) and recovery (> 99%).[97] Block copolymers containing a SA block also show improved shape recovery performance.[113]

Hydrogels incorporating an s-SVP like hydrophobic moiety have also been investigated for high strain and shape recovery. In these shape memory phase-separated organohydrogels, the phase-transition micro-organogels and elastic hydrogel framework act synergistically to provide good thermomechanical performance and reversible shape change effect. The organohydrogels were prepared by in situ polymerizations of an emulsion system that contained hydrophilic N, N-dimethyl acrylamide (DMA) and lauryl methacrylate (**Figure** 7b).[102] Covalent interactions at the interface between the oil and aqueous phases, as well as the surface tension of the micro-organogel particles in the oil phase, were shown to significantly enhance the toughness of the resulting organohydrogel material. Due to the synergistic effects, the s-SVP based organohydrogels exhibit very high strain capacity, featuring fully recoverable stretching deformation by up to 2600%. The same research group further replaced lauryl methacrylate with SMA to fabricate a biphasic synergistic gel.[103] The switchable mechanics derived from its heterostructure elicit high stiffness and large strain shape programming. The interfacial tension of the heterostructures improves the shape recovery.[114]

Other hydrogels, such as poly(acrylamide) (PAAm),[100, 105, 115, 116] poly(acrylic acid) (PAA),[117, 118] and poly(N-isopropyl acrylamide) (PNIPAM),[119] are also added to increase the reversible shape transformation performance. Since s-SVP with a long alkyl chain is normally hydrophobic, emulsifiers such as sodium dodecyl sulfate,[117] nanoclay,[102] gelatin,[120] and

AlOOH nanoparticles[100] are necessary to stabilize the s-SVP based organohydrogels. Functional materials, such as a small amount of gold nanoparticles, can be included in the stearyl acrylate-based organohydrogel. The gold nanoparticle-containing hydrogel exhibits a light-responsive shape memory effect due to the photothermal effect of the nanoparticles.[121]

As SMPs, the s-SVPs 'memorize' one temporary state that they are programmed to in addition to their original shape. They typically lack sophisticated programmability for complicated shape-encoding behaviors and mechanics. A second stimulus-responsive component with modulus tuning functionality can be incorporated for multiple programmable shapes. The key is to implant a second shape morphing mechanism that demonstrates reversible physical or chemical interaction for modulus adjustment. Zhang *et al.*, introduced reversible ionic coordination bonding Fe^{3+}-AA, a species of supramolecular interaction, into the SA/acrylamide-based organohydrogel to fabricate mechanically robust stiffness variable polymers.[118] Due to the unique dual-programmability of the orthogonal supramolecular hetero-networks, this approach was also investigated to demonstrate hierarchical shape morphing behavior that enables the step-wise execution of sophisticated origami, kirigami, and multidimensional shape changes far exceeding conventional shape morphing capacity.[105] Reversible hydrogen bonds could also be employed in the s-SVP system to enable multiple shape transformations. For instance, AA and quaternary chitosan (QCH), two chemical species that exhibit reversible electrostatic interaction, were incorporated into the SMA system.[122] As shown in Figure 7c, due to the reversible nature of the hydrogen bonding between AA and QCH together with the hydrophobic interactions of alkyl chains in SMA, the organohydrogel exhibits superior fatigue resistance and has shape memory effect in response to a variety of stimuli, such as temperature, pH and NaCl solution. The synergistic effects of different noncovalent bonds associated with one s-SVP system render more programmable organohydrogels. Change et *al*. prepared a series of tough films by polymerizing SA with ureidopyrimidone (UPy) and AA.[123] The thermally responsive UPy motifs dimerized with quadruple hydrogen bonds, reversible metal-coordination interactions between metal ions (Ca^{2+}, Fe^{3+}) and carboxyl acid groups in AA, and the phase change of the long alkyl chains make the resultant organohydrogel a triple-shape memory polymer.

4.1.3 Applications based on Reversible Shape Transformation

S-SVP organohydrogels exhibiting reversible shape transformation could be employed in soft robotics. A 3D-printed s-SVP based actuator was used as an underwater 3D macroscopic soft gripper that could grab, transport, and release a guest object.[114] Programmable

organohydrogels with multistable mechanical states were constructed by an on-demand modular assembly of noneutectic phase transition components inside microrganogel inclusions,[100] which results in a precisely controllable multi-step switching mechanism. The organohydrogel was used to design a soft gripper with adaptive grasping through stiffness matching with various objects via pneumatic-thermal hybrid actuation (Figure 7d). Examples of other soft robotic manipulators include octopus-inspired robotic tentacles and liquid transporters. A dual-programmable s-SVP based supramolecular organohydrogel was used to achieve on-demand control of spontaneously unidirectional liquid transportation.[105] Likewise, inspired by the functional surface of the pitcher plant and the rice leaf, a poly(SMA) based superamphiphilic organohydrogel with reconfigurable surface topography was constructed for programming unidirectional liquid transport.[115] Through the reconfiguration of its hetero-network surface, this organohydrogel can spread different liquids in multiphase environments, which could provide a platform to conduct catalytic microreactions, deliver drugs without an external power source, and provide self-lubrication.

4.2. Bistable Electro-mechanical Transduction

4.2.1 Mechanism of Bistable Electro-mechanical Transduction

Dielectric elastomers have emerged as a class of electroactive material exhibiting large actuation strain induced by electrostatic stress under an external electric field (**Figure 8**a). A low elastic modulus is essential to obtain a large actuation strain and high energy density.[124-127] The low elastic modulus, however, limits the material's capability for load-bearing. In addition, the voltage needs to be continuously applied to maintain the deformed shape, which consumes energy and reduces device lifetime. We have been exploring the combination of shape memory property with dielectric elastomers for bistable actuation.[128] Figure 8b illustrates the operation of such a bistable electroactive polymer (BSEP). At room temperature, the BSEP behaves like a rigid plastic. Above its transition temperature, it enters the soft state and can be actuated like a dielectric elastomer. Once the temperature is reduced below the transition temperature, the bias voltage can be removed and the actuated deformation is preserved. The BSEP can thus be actuated to various stable shapes. The original shape can be recovered by heating the polymer above the transition temperature.

4.2.2 Materials for Bistable Electro-mechanical Transduction

The first BSEP polymer demonstrated is poly(tert-butyl acrylate) (PTBA), which is thermoplastic and semicrystalline. The glass transition of the amorphous domain is used for

shape programming and memory, while the nanocrystallites serve as the netpoints. The maximum actuation strain obtained was 335% of area expansion at 260 MV/m.[128] Due to the non-uniformity of the nanocrystallite size and melting points, the modulus of the thermoplastic PTBA continuously decreases with increasing temperature above the glass transition, leading to nonuniform and unstable actuation. Introducing chemical crosslinks alleviated the instability, though the glass transition temperature range was still rather broad.[129]

The large modulus change, narrow transition temperature span, and high density of chemical crosslinks make the s-SVP an interesting candidate for the BSEP. The super-soft state of the s-SVP when heated is also significantly beneficial for the actuation performance. Furthermore, the transition temperature of s-SVP could be tuned to around human body temperature, which is desirable in wearable applications. **Figure 9**a shows the bistable actuation of the s-SVP based on SA: UDA = 60:40.[52] The diaphragm actuator based on the polymer thin film was electrically actuated up to 70% strain at 127 MV/m in the soft state.

4.2.3 Applications based on Bistable Electro-mechanical Transduction

The bistability of the BSEP actuation is suitable for haptic applications. There have been extensive efforts to develop compact Braille electronic books, though the high driving voltage for the dielectric elastomer actuation at the softened state poses practical challenges. [130, 131] Pneumatic actuation was thus introduced that allows the Braille panel to be operated at a low voltage. Figure 9b illustrates a refreshable Braille panel fabricated with the s-SVP based BSEP membrane and a pneumatic pump. The s-SVP demonstrated a steep modulus change of 1000-fold over a temperature range of 6 °C such that the rigid state can support the finger-pressing force as required by Braille standard, and the soft state can be actuated by a thumb-size pump. The diaphragm pixels were patterned with a 2.5 mm pitch to meet this standard. The out-of-plane displacement of the diaphragms is up to 0.7 mm.[104] Applying 30 V could raise the temperature of the BSEP to 50 ºC in less than 1 s for the pneumatic actuation. In comparison, the commercial SMP MM4520 exhibits a 100-fold variation in stiffness over 20 °C.

The s-SVP based BSEP actuators can also modulate photonic crystals embedded in the elastomer, which enables an electric field to control reflectance and transmittance properties (Figure 9c).[132] A rewritable inkless paper was demonstrated by incorporating ferroferric oxide-carbon (Fe_3O_4@C) core-shell nanoparticles (NPs) in the BSEP matrix photopolymerized from SA and UDA. The magnetic photonic crystal was dispersed in the liquid monomer and aligned with a magnetic field before the photopolymerization. This method has compelling potential as a display technology forming the basis of soft, wearable displays with low power requirements.

Wang *et* al. developed a bistable out-of-plane dielectric elastomer actuator by adopting a bilayer structure made from BSEP and a passive layer, as illustrated in Figure 9d.[133] The BSEP film was synthesized by photopolymerizing SA with soft segment AC9307. Through adjusting the reactant ratio, its phase-transition point can be tuned around ambient temperature. This as-prepared actuator is able to maintain its actuated shape at a large bending angle without continuously applied stimuli when it is at the cold state.

4.3. Optical Modulation

4.3.1 Mechanism of Optical Modulation

Optical modulation is useful for privacy protection, solar irradiation regulation, anticounterfeiting/camouflage, and display technologies.[134, 135] Thermoresponsive materials are attractive for optical modulation, as the different colors or optical transmittance could be triggered by Joule heating or automatically through environmental temperature changes. Autonomous modulation is particularly interesting as it is simple, energy-efficient, and cost-effective. The semicrystalline-amorphous phase change of the s-SVP has been explored for reversible and fast opaque-transparent switching. Above its melting temperature, an s-SVP is transparent with long alkyl chains forming homogeneous, random coils in a uniformly-distributed manner. The molar volume of this amorphous polymer, V_a, is approximately 1.60 times its van der Waals volume V_w.[136] Below crystallization temperature, the molar volume of the crystalline region, V_c, decreases to about 1.43 times that of V_w, representing a ~10% volume reduction. According to the Lorentz–Lorenz Equation, there would consequently be an increase in the refractive index.[137] A mismatch of the refractive index between the crystalline regions and the continuous amorphous phase in the semicrystalline s-SVP would, therefore, lead to light scattering and make the s-SVP opaque below its transition temperature, as shown in **Figure 10**a.

In order to modulate the transparency of the s-SVP, parameters including crystallite size, crystallinity%, and refractive index are considered. In general, the crystallization of side-chains has limited crystallite size, typically of nanometer scales.[67] Taking the representative s-SVP poly(SA) as an example, its x-ray diffraction peak angle and full width at half max (FWHM) indicate crystallite size being between 3.53 and 4.36 nm, according to the Scherrer equation.[67, 138] The aggregation of the nanocrystals leads to crystalline-rich and amorphous-rich regions up to a few hundred nanometers,[139, 140] and thus deteriorates the transparency. If the nanocrystallites are confined in nanostructures[141-143] well below the wavelength of visible light, around 1/15 of the visible wavelength or roughly 600/15 = 40 nm, light scattering can be largely eliminated, resulting in a transparent material.[144] On the contrary, if increasing the size of the

crystalline domains or introducing micro-size phase separation in the polymer, light scattering would be enhanced.[145, 146] Here, light scattering can either be Mie scattering when domains are similar to, or larger than the wavelength, or Rayleigh scattering when domains are small with respect to wavelengths of light.[147, 148] Crystallinity%, the volume ratio of crystalline and amorphous regions, also affects the s-SVP's transparency.

4.3.2 Materials and Applications for Optical Modulation

The s-SVPs are interesting candidates for optical modulation thanks to their high crystallinity% and narrow transition span. The transition temperature of s-SVPs could be adjusted to conform with human sensory thermoneutral (normally in the range of 30–34°C).[149] We added a poly(ethylene oxide) oligomer to crosslink with poly(SA), leading to micro-sized surface patterns in the resulting s-SVP and an increase of opacity at ambient temperature (Figure 10b).[138] The refractive indices of the crystalline poly(SA) domain and the polyethylene oxide domain are mismatched. When the poly(SA) domain melts, its amorphous state matches the polyethylene oxide domain in the refractive index. The s-SVP is thus transparent at elevated temperatures. The temperature change could be administered with an embedded Joule heating electrode which is transparent. For autonomous opacity change as a smart window, we developed a new s-SVP that stays transparent at room temperature, allowing sunlight to pass through, and turns opaque above 32 °C to block solar radiation as illustrated in Figure 10c.[150] This reversal of the opacity change in the new s-SVP was achieved by replacing the polyethylene oxide oligomer with hydroxyethyl acrylate. The resulting copolymer forms a phase-separated microstructure with hydrophilic poly(hydroxyethyl acrylate) phase that matches the semicrystalline poly(hexadecyl acrylate) domain in refractive index. The copolymer film has an optical transmittance of 80.9% in the visible wavelength range at ambient temperature. Above 32 °C, as the poly(hexadecyl acrylate) domain melts, the index matching is broken, and the transmittance declines to 12.1%. The micrometer-sized phase separation behavior renders broadband optical modulation from visible to infrared spectrum through the reversible phase change of the ply(hexadecyl acrylate) phase. By adding tetradecyl acrylate, the transition temperature may be adjusted. Crosslinking density also affects the opacity. Lower crosslink density leads to higher crystallinity% due to less constraint in molecular mobility.

Deng *et al.* developed a dual-mode temporal communicator via digitally programmable s-SVP (Figure 10d).[151] In the system, a pixelated polymer is synthesized by photo-curing SA with 1,6-hexanediol diacrylate under different doses of light exposure, which gives rise to a

network with spatially-distributed crosslinking density. The as-prepared polymer film was utilized as a programmable time-encrypted device for the communication of time-specific optical information.

4.4. Reversible Adhesion

4.4.1 Mechanism of Reversible Adhesion

Adhesives that enable bonding and debonding on demand (DoD) broaden the functionalities of adhesives in connection with temporal fixation, repair, and recycling.[31, 152-156] Indeed, reversible adhesives are under development for wound dressing,[157] epidermal electronics,[158] and temporal fixation in semiconductor manufacturing.[159] SVPs are obvious choices thanks to their temperature-controlled modulus changes. For the SVPs having crystallizable segments in the backbone, such as polyether group crosslinked in isocyanate-hydroxyl reaction group[19] and epoxy-amine reaction group[160, 161] formed networks, the phase-changing segments have limited mobility that may affect the adhesive's ability to form highly conforming and strong-bonding interfaces with the substrate. They may also re-crystallize to detach from the substrate. In the s-SVPs, the long alkyl chains dangling on the backbone have both high regularity and flexibility, giving the side chains high mobility for high crystallinity% along with a narrow transition temperature range, efficient transition rate, and large modulus difference. These advantageous features collectively impart the s-SVP with well-behaved reversible adhesion (**Figure 11**a). When an s-SVP film is physically attached to an adherend, the polymer chains exhibit an intrinsic work of adhesion, or surface energy W_{ad}. Meanwhile, the film around the interface will be highly deformed, thus dissipating a significant amount of mechanical energy and contributing to the dissipation energy W_{dis}. The total peeling energy (W) of the s-SVP/adherend bonding can be expressed as[162, 163]

$$W = W_{ad} + W_{dis} \quad (4)$$

Among which, W_{dis} can be evaluated as [163]

$$W_{dis} = \sigma^2 V / 2E \quad (5)$$

Where σ is the applied stress, V is the volume for storing the dissipation energy, and E is the elastic modulus of the s-SVP film. For a highly compliant adhesive, the W_{dis} is normally much larger than W_{ad} and dominates the peeling energy.[164] The dissipation energy W_{dis} is inversely proportional to the DoD adhesive's modulus. When below its transition temperature, the high E value of the s-SVP leads to low W_{dis}, and the surface energy W_{ad} becomes significant to the s-SVP film's peel strength, although it remains a very low value. When the film is heated above the transition temperature, its low modulus and large deformation result in high values of

dissipation energy W_{dis} and therefore, high peeling energy. The adhesion energy is dissipated well into the bulk of the s-SVP film.

4.4.2 Materials and Applications for Reversible Adhesion

The adhesive property above its transition temperature renders s-SVP a well-behaved epidermal substrate for wearable electronics. Qiu *et al*. developed a highly sensitive capacitive touch sensor on a self-conformable s-SVP based substrate fabricated by copolymerizing SA, UDA, and AA.[165] The s-SVP polymer's strong adhesion grants sensors the ability to conform to the shape of various surfaces under different working conditions. The variable adhesion strengths of the s-SVP were utilized to demonstrate a wearable device where on-demand bonding and debonding were triggered by skin temperature. It is like a DoD sticker for a wearable self-powered mechanosensitive communication system, as shown in Figure 11b.[50] The sticker is made of a copolymer comprising of SA and TA in a chemically crosslinked urethane diacrylate elastomer network. The crystalline melting transition of the mixed stearyl and tetradecyl chains between 26 °C and 32°C leads to a large modulus reduction and high flowability. The sticker is sticky above 32 °C, allowing E-skins to adhere to skin and stay attached during routine activities. It becomes non-tacky and easily removable from the skin at temperatures below 26°C, which is accessible by simply using tap water. This DoD adhesive allows repeated usage with negligible damage to the skin.

5. Summary and Outlook

The s-SVPs can be synthesized via the bulk copolymerization of acrylates containing a long normal alkyl chain and a network-forming acrylate dimer or oligomer. The resulting polymers resemble crosslinked bottlebrush polymers with high-graft density but limited graft length (typically 14-18 carbons in the alkyl chains). These s-SVPs are highly crystalline with a narrow melting range. The crosslinks render the s-SVPs a rubbery elastomer above the transition temperature. The transition from a rigid plastic (modulus ~ 10^2 MPa) state to a super-soft rubbery (~ 10^{1-2} kPa) state can be quickly completed and reversed. The sharp phase change has been explored for a number of applications, including reversible shape transformation, bistable electro-mechanical transduction, optical modulation, and reversible adhesion.

The bulk polymerization makes it feasible to introduce other functional components into the s-SVP matrix. Incorporating a water-responsive hydrogel or cellulose nanofibers afford composites that are dual responsive to both temperature and moisture changes. In the case of using cellulose nanofiber fillers, the modulus change can be enhanced to 24,000-fold, from

around 1 GPa to 40 kPa. Embedding a photonic crystal in the s-SVP leads to an ink-free rewritable paper that one may write on with a finger press or a driving circuit. We anticipate further developments in this avenue by introducing other functional additives.

New research may also be directed to further widen the range of available stiffness, narrow the transition temperature span, and identify new graft structures with different transition temperatures that the normal alkyl chains can offer. While the modulus of the s-SVP in a super-soft state is on the same order of magnitude as soft tissues, the rigid state is far inferior to bones with regard to load-bearing. It would be interesting to investigate polar side groups for larger enthalpy change in the crystal melting. Moieties that form reversible chemical bonding are also of interest to build s-SVPs with greater modulation. Variable modulus has been demonstrated in systems containing Diels-Alder cycloaddition pairs, though the broad reaction temperature ranges in both forward and reverse reactions limits the modulus change ratio to a single digit. We note that the Diels-Alder cycloaddition has been well developed for self-healing of cracks. Incorporating other reversible bonds, such as the disulfide bond or metal-carboxylate coordination bond, points to a new avenue for developing healable stiffness variable materials.

There should be significant room for further improvement of the s-SVP for engineering applications, including the phase-changing alkyl side chain lengths, graft uniformity via block polymerization, nature and density of the crosslinks, and segment lengths. The design of experiments (DOE) and machine learning (ML) could be useful tools to quickly optimize the s-SVPs. The developed s-SVPs may find applications in areas such as haptic interface, prosthetic limb, wearable assistive device, and implantable devices. Advanced fabrication methods, like 3D printing and soft lithography, could be used to increase the micro- and macrostructural diversity of s-SVP for these devices. The development of s-SVP has led to a range of thermo-responsive polymeric systems; however, challenges remain for the implementation of high-resolution spatial heat generation for operation convenience or behavioral complexity.

Acknowledgements

The authors wish to acknowledge partial finance support by the Office of Naval Research (award no. N00014-19-1-2212). The authors thank Claire Shen from UCLA for revising the manuscript.

Conflict of Interest

The authors declare no conflict of interest.

Received: ((will be filled in by the editorial staff))
Revised: ((will be filled in by the editorial staff))
Published online: ((will be filled in by the editorial staff))

Author biographies

Meng Gao is currently an assistant professor at Tianjin University of Science and Technology. She received her PhD from Institute of Chemistry, Chinese Academy of Sciences. She was a postdoctoral fellow in Materials Science and Engineering and Mechanical Engineering at the University of California, Los Angeles. She specializes in printing electronics and photonic devices.

Yuan Meng is currently a postdoctoral scholar in Materials Science and Engineering at the University of California, Los Angeles. He earned his PhD at University of Rochester, majoring in Chemical Engineering. Yuan is interested broadly in smart materials, stretchable electronics, and polymer physics. His current project involves electrocaloric cooling device design and artificial muscle fabrication.

Claire Shen is currently a 4th year undergraduate student studying Materials Science and Engineering at the University of California, Los Angeles. She is currently a research assistant at the Soft Materials Laboratory lead by Professor Qibing Pei working on dielectric elastomer actuators (DEAs).

Qibing Pei is Professor of Materials Science and Engineering and Mechanical Engineering at the University of California, Los Angeles, and directs the UCLA Soft Materials Research Laboratory. He specializes in synthetic polymers and composites for electronic, electromechanical, and photonic applications. He received a PhD from the Institute of Chemistry, Chinese Academy of Sciences. He was a postdoctoral fellow in Linköping University and worked at UNIAX Corporation (DuPont Display) and SRI International. He is a Fellow of SPIE, member of ACS and MRS, Advisory Board Member of Smart Materials & Structures, Soft Robotics, and Advanced Electronic Materials.

References

[1] I. A. Kinloch, J. Suhr, J. Lou, R. J. Young, P. M. Ajayan, *Science* **2018**, *362*, 547.

[2] S. Chen, L. Sun, X. Zhou, Y. Guo, J. Song, S. Qian, Z. Liu, Q. Guan, E. Meade Jeffries, W. Liu, Y. Wang, C. He, Z. You, *Nat. Commun.* **2020**, *11*, 1107.

[3] L. Montero de Espinosa, W. Meesorn, D. Moatsou, C. Weder, *Chem. Rev.* **2017**, *117*, 12851.

[4] D. Rus, M. T. Tolley, *Nature* **2015**, *521*, 467.

[5] M. A. C. Stuart, W. T. S. Huck, J. Genzer, M. Müller, C. Ober, M. Stamm, G. B. Sukhorukov, I. Szleifer, V. V. Tsukruk, M. Urban, F. Winnik, S. Zauscher, I. Luzinov, S. Minko, *Nat. Mater.* **2010**, *9*, 101.

[6] Q. Pei, *Soft Rob.* **2016**, *3*, 1.

[7] L. Blanc, A. Delchambre, P. Lambert, *Actuators* **2017**, *6*, 23.

[8] F. Thurmond, J. Trotter, *J. Exp. Biol.* **1996**, *199*, 1817.

[9] J. R. Capadona, K. Shanmuganathan, D. J. Tyler, S. J. Rowan, C. Weder, *Science* **2008**, *319*, 1370.

[10] P. Fratzl, F. G. Barth, *Nature* **2009**, *462*, 442.

[11] A. Gollhofer, D. Schmidtbleicher, V. Dietz, *Int. J. Sports Med.* **1984**, *05*, 19.

[12] T. Sinkjaer, E. Toft, S. Andreassen, B. C. Hornemann, *J. Neurophysiol.* **1988**, *60*, 1110.

[13] J. Mohd Jani, M. Leary, A. Subic, M. A. Gibson, *Mater. Des.* **2014**, *56*, 1078.

[14] I. K. Kuder, A. F. Arrieta, W. E. Raither, P. Ermanni, *Progress in Aerospace Sciences* **2013**, *63*, 33.

[15] T. Daeneke, K. Khoshmanesh, N. Mahmood, I. A. de Castro, D. Esrafilzadeh, S. J. Barrow, M. D. Dickey, K. Kalantar-zadeh, *Chem. Soc. Rev.* **2018**, *47*, 4073.

[16] A. G. Olabi, A. Grunwald, *Mater. Des.* **2007**, *28*, 2658.

[17] Z. G. Wei, R. Sandstroröm, S. Miyazaki, *J. Mater. Sci.* **1998**, *33*, 3743.

[18] I. Apsite, A. Biswas, Y. Li, L. Ionov, *Adv. Funct. Mater.* **2020**, *30*, 1908028.

[19] J. K. Park, K. Nan, H. Luan, N. Zheng, S. Zhao, H. Zhang, X. Cheng, H. Wang, K. Li, T. Xie, Y. Huang, Y. Zhang, S. Kim, J. A. Rogers, *Advanced Materials* **2019**, *31*, 1905715.

[20] R. Liang, H. Yu, L. Wang, B. U. Amin, N. Wang, J. Fu, Y. Xing, D. Shen, Z. Ni, *Chem. Mater.* **2021**, *33*, 1190.

[21] C. S. Brazel, S. L. Rosen, *Fundamental principles of polymeric materials*, John Wiley & Sons, 2012.

[22] Y.-L. Liu, T.-W. Chuo, *Polym. Chem.* **2013**, *4*, 2194.

[23] J. Li, J. Liang, L. Li, F. Ren, W. Hu, J. Li, S. Qi, Q. Pei, *ACS Nano* **2014**, *8*, 12874.

[24] W. Hu, Z. Ren, J. Li, E. Askounis, Z. Xie, Q. Pei, *Adv. Funct. Mater.* **2015**, *25*, 4827.

[25] D. Aoki, Y. Teramoto, Y. Nishio, *Biomacromolecules* **2007**, *8*, 3749.

[26] H. Meng, P. Xiao, J. Gu, X. Wen, J. Xu, C. Zhao, J. Zhang, T. Chen, *Chem. Commun.* **2014**, *50*, 12277.

[27] H. Xiao, W. Lu, X. Le, C. Ma, Z. Li, J. Zheng, J. Zhang, Y. Huang, T. Chen, *Chem. Commun.* **2016**, *52*, 13292.

[28] X. Hu, J. Zhou, M. Vatankhah-Varnosfaderani, W. F. M. Daniel, Q. Li, A. P. Zhushma, A. V. Dobrynin, S. S. Sheiko, *Nat. Commun.* **2016**, *7*, 12919.

[29] J. Yang, R. Bai, Z. Suo, *Adv. Mater.* **2018**, *30*, 1800671.

[30] X.-J. Han, Z.-Q. Dong, M.-M. Fan, Y. Liu, J.-H. li, Y.-F. Wang, Q.-J. Yuan, B.-J. Li, S. Zhang, *Macromol. Rapid Commun.* **2012**, *33*, 1055.

[31] Y. Gao, K. Wu, Z. Suo, *Adv. Mater.* **2019**, *31*, 1806948.

[32] R. D. Harris, J. T. Auletta, S. A. M. Motlagh, M. J. Lawless, N. M. Perri, S. Saxena, L. M. Weiland, D. H. Waldeck, W. W. Clark, T. Y. Meyer, *ACS Macro Letters* **2013**, *2*, 1095.

[33] W. Nan, W. Wang, H. Gao, W. Liu, *Soft Matter* **2013**, *9*, 132.

[34] Q. Zhao, H. J. Qi, T. Xie, *Prog. Polym. Sci.* **2015**, *49-50*, 79.

[35] A. Biswas, A. P. Singh, D. Rana, V. K. Aswal, P. Maiti, *Nanoscale* **2018**, *10*, 9917.

[36] J. Dong, R. A. Weiss, *Macromolecules* **2011**, *44*, 8871.

[37] R. Dolog, R. A. Weiss, *Macromolecules* **2013**, *46*, 7845.

[38] A. Biswas, V. K. Aswal, P. Maiti, *J. Colloid Interface Sci.* **2019**, *556*, 147.

[39] Z. Wen, K. Yang, J.-M. Raquez, *Molecules* **2020**, *25*, 1241.

[40] D. L. Safranski, J. C. Griffis, *Shape-memory polymer device design*, William Andrew, 2017.

[41] Y. Xia, Y. He, F. Zhang, Y. Liu, J. Leng, *Advanced Materials* **2021**, *33*, 2000713.

[42] H. Y. Liang, B. J. Morgan, G. J. Xie, M. R. Martinez, E. B. Zhulina, K. Matyjaszewski, S. S. Sheiko, A. V. Dobrynin, *Macromolecules* **2018**, *51*, 10028.

[43] S. S. Sheiko, A. V. Dobrynin, *Macromolecules* **2019**, *52*, 7531.

[44] H. Y. Liang, Z. Cao, Z. L. Wang, S. S. Sheiko, A. V. Dobrynin, *Macromolecules* **2017**, *50*, 3430.

[45] W. F. M. Daniel, J. Burdyńska, M. Vatankhah-Varnoosfaderani, K. Matyjaszewski, J. Paturej, M. Rubinstein, A. V. Dobrynin, S. S. Sheiko, *Nat. Mater.* **2016**, *15*, 183.

[46] T. Pakula, Y. Zhang, K. Matyjaszewski, H.-i. Lee, H. Boerner, S. Qin, G. C. Berry, *Polymer* **2006**, *47*, 7198.

[47] D. Neugebauer, M. Theis, T. Pakula, G. Wegner, K. Matyjaszewski, *Macromolecules* **2006**, *39*, 584.

[48] D. Neugebauer, Y. Zhang, T. Pakula, S. S. Sheiko, K. Matyjaszewski, *Macromolecules* **2003**, *36*, 6746.

[49] W. F. M. Daniel, G. J. Xie, M. V. Varnoosfaclerani, J. Burdynska, Q. X. Li, D. Nykypanchuk, O. Gang, K. Matyjaszewski, S. S. Sheiko, *Macromolecules* **2017**, *50*, 2103.

[50] M. Gao, H. Wu, R. Plamthottam, Z. Xie, Y. Liu, J. Hu, S. Wu, L. Wu, X. He, Q. Pei, *Matter* **2021**, *4*, 1962.

[51] M. Vatankhah-Varnosfaderani, W. F. M. Daniel, M. H. Everhart, A. A. Pandya, H. Y. Liang, K. Matyjaszewski, A. V. Dobrynin, S. S. Sheiko, *Nature* **2017**, *549*, 497.

[52] Z. Ren, W. Hu, C. Liu, S. Li, X. Niu, Q. Pei, *Macromolecules* **2016**, *49*, 134.

[53] Y. Kagami, J. P. Gong, Y. Osada, *Macromol. Rapid Commun.* **1996**, *17*, 539.

[54] Y. Zheng, M. L. Bruening, G. L. Baker, *Macromolecules* **2007**, *40*, 8212.

[55] Y. Zheng, M. L. Bruening, G. L. Baker, *J. Polym. Sci., Part B: Polym. Phys.* **2010**, *48*, 1955.

[56] H. L. Sun, D. M. Yu, S. W. Shi, Q. Q. Yuan, S. Fujinami, X. L. Sun, D. Wang, T. P. Russell, *Macromolecules* **2019**, *52*, 592.

[57] T. Hirabayashi, T. Kikuta, K. Kasabou, K. Yokota, *Polym. J.* **1988**, *20*, 693.

[58] H. Q. Mao, H. X. Wang, J. Li, L. Zhang, J. Y. Shi, H. F. Shi, *Polymer* **2020**, *202*.

[59] H. S. Kaufman, A. Sacher, T. Alfrey, I. Fankuchen, *J. Am. Chem. Soc.* **1948**, *70*, 3147.

[60] N. A. Plate, V. P. Shibaev, B. S. Petrukhin, Y. A. Zubov, V. A. Kargin, *J. Polym. Sci. A‐1 Polym. Chem.* **1971**, *9*, 2291.

[61] A. Matsuda, J. Sato, H. Yasunaga, Y. Osada, *Macromolecules* **1994**, *27*, 7695.

[62] C. L. Lewis, Y. Meng, M. Anthamatten, *Macromolecules* **2015**, *48*, 4918.

[63] Y. Meng, J. Jiang, M. Anthamatten, *J. Polym. Sci. B: Polym. Phys* **2016**, *54*, 1397.

[64] S. A. Greenberg, T. Alfrey, *J. Am. Chem. Soc.* **1954**, *76*, 6280.

[65] K. Kunal, C. G. Robertson, S. Pawlus, S. F. Hahn, A. P. Sokolov, *Macromolecules* **2008**, *41*, 7232.

[66] M. Beiner, K. Schröter, E. Hempel, S. Reissig, E. Donth, *Macromolecules* **1999**, *32*, 6278.

[67] M. Beiner, H. Huth, *Nat. Mater.* **2003**, *2*, 595.

[68] C. L. Jackson, G. B. McKenna, *J. Non-Cryst. Solids* **1991**, *131-133*, 221.

[69] A. Huwe, F. Kremer, P. Behrens, W. Schwieger, *Phys. Rev. Lett.* **1999**, *82*, 2338.

[70] M. Arndt, R. Stannarius, H. Groothues, E. Hempel, F. Kremer, *Phys. Rev. Lett.* **1997**, *79*, 2077.

[71] J. M. G. Cowie, Z. Haq, I. J. McEwen, J. Velićkovič, *Polymer* **1981**, *22*, 327.

[72] K. W. McCreight, J. J. Ge, M. Guo, I. Mann, F. Li, Z. Shen, X. Jin, F. W. Harris, S. Z. D. Cheng, *J. Polym. Sci., Part B: Polym. Phys.* **1999**, *37*, 1633.

[73] R. Böhmer, K. L. Ngai, C. A. Angell, D. J. Plazek, *J. Chem. Phys.* **1993**, *99*, 4201.

[74] Y. Jian, Y. He, J. Wang, W. Yang, J. Nie, *Polym. Int.* **2013**, *62*, 1692.

[75] Y. Jian, Y. He, J. Wang, B. Xu, W. Yang, J. Nie, *New J. Chem.* **2013**, *37*, 444.

[76] Q. Lian, K. Li, A. A. S. Sayyed, J. Cheng, J. Zhang, *J. Mater. Chem. A* **2017**, *5*, 14562.

[77] H. Xu, Y. Gao, J. Li, H. Wang, H. Shi, *Polymer* **2018**, *153*, 362.

[78] L. J. Li, H. F. Shi, X. X. Zhang, *Adv. Mater. Res.* **2012**, *482*, 1921.

[79] H. Wang, X. Han, H. Shi, X. Zhang, L. Qi, D. Wang, *CrystEngComm* **2014**, *16*, 7090.

[80] K. Inomata, E. Nakanishi, Y. Sakane, M. Koike, T. Nose, *J. Polym. Sci., Part B: Polym. Phys.* **2005**, *43*, 79.

[81] F. Yang, P. Déjardin, Y. Frère, P. Gramain, *Makromol. Chem.* **1990**, *191*, 1209.

[82] W. Miao, W. Zou, B. Jin, C. Ni, N. Zheng, Q. Zhao, T. Xie, *Nat. Commun.* **2020**, *11*, 4257.

[83] Y.-J. Heo, H.-G. Jeong, J. Kim, B. Lim, J. Kim, Y. Kim, B. Kang, J.-M. Yun, K. Cho, D.-Y. Kim, *ACS Appl. Mater. Interfaces* **2020**, *12*, 49886.

[84] H. Li, W. Gu, L. Li, Y. Zhang, T. P. Russell, E. B. Coughlin, *Macromolecules* **2013**, *46*, 3737.

[85] M. Morita, H. Ogisu, M. Kubo, *J. Appl. Polym. Sci.* **1999**, *73*, 1741.

[86] H. Yamaguchi, M. Kikuchi, M. Kobayashi, H. Ogawa, H. Masunaga, O. Sakata, A. Takahara, *Macromolecules* **2012**, *45*, 1509.

[87] Q. Zhang, Q. Wang, J. Jiang, X. Zhan, F. Chen, *Langmuir* **2015**, *31*, 4752.

[88] N. A. Platé, V. P. Shibaev, *J. Polym. Sci.: Macromol. Rev.* **1974**, *8*, 117.

[89] D. Zanuy, D. A. Zazueta, C. Alemán, *Polymer* **2003**, *44*, 4735.

[90] H. Shi, Y. Zhao, S. Jiang, J. H. Xin, J. Rottstegge, D. Xu, D. Wang, *Polymer* **2007**, *48*, 2762.

[91] H. Shi, Y. Zhao, S. Jiang, J. Rottstegge, J. H. Xin, D. Wang, D. Xu, *Macromolecules* **2007**, *40*, 3198.

[92] W.-Y. Zheng, K. Levon, J. Laakso, J.-E. Oesterholm, *Macromolecules* **1994**, *27*, 7754.

[93] S. Livshin, M. S. Silverstein, *Macromolecules* **2007**, *40*, 6349.

[94] E. Hempel, H. Huth, M. Beiner, *Thermochim. Acta* **2003**, *403*, 105.

[95] Y. Shibasaki, H. Saitoh, K. Chiba, *J. Therm. Anal.* **1997**, *49*, 115.

[96] H. Mao, Y. Wang, H. Wang, L. Li, H. Shi, *Polym. Int.* **2021**, DOI:10.1002/pi.6283.

[97] H. Du, J. Marin Angel, S. Basak, T.-Y. Lai, K. A. Cavicchi, *Macromol. Rapid Commun.* **2021**, *42*, 2100072.

[98] E. Su, C. Bilici, G. Bayazit, S. Ide, O. Okay, *ACS Appl. Mater. Interfaces* **2021**, *13*, 21786.

[99] Q. Lian, Y. Li, A. A. S. Sayyed, J. Cheng, J. Zhang, *ACS Sustain. Chem. Eng.* **2018**, *6*, 3375.

[100] S. Zhuo, Z. Zhao, Z. Xie, Y. Hao, Y. Xu, T. Zhao, H. Li, E. M. Knubben, L. Wen, L. Jiang, M. Liu, *Sci. Adv.* **2020**, *6*, 1464.

[101] Y. Qiu, E. Askounis, F. Guan, Z. Peng, W. Xiao, Q. Pei, *ACS Appl. Polym. Mater.* **2020**, *2*, 2008.

[102] Z. Zhao, K. Zhang, Y. Liu, J. Zhou, M. Liu, *Adv. Mater.* **2017**, *29*, 1701695.

[103] Z. Zhao, Y. Liu, K. Zhang, S. Zhuo, R. Fang, J. Zhang, L. Jiang, M. Liu, *Angew. Chem.* **2017**, *129*, 13649.

[104] Q. Yu, L. Zhiyun, P. Qibing, *ACS Appl. Mater. Interfaces* **2018**, *10*, 24807.

[105] Z. Zhao, S. Zhuo, R. Fang, L. Zhang, X. Zhou, Y. Xu, J. Zhang, Z. Dong, L. Jiang, M. Liu, *Adv. Mater.* **2018**, *30*, 1804435.

[106] M. Behl, A. Lendlein, *Mater. Today* **2007**, *10*, 20.

[107] P. T. Mather, X. Luo, I. A. Rousseau, *Annu. Rev. Mater. Res.* **2009**, *39*, 445.

[108] H. Meng, G. Li, *Polymer* **2013**, *54*, 2199.

[109] A. Lendlein, O. E. C. Gould, *Nat. Rev. Mater.* **2019**, *4*, 116.

[110] B. Wu, H. Lu, X. Le, W. Lu, J. Zhang, P. Théato, T. Chen, *Chem. Sci.* **2021**, *21*, 6472.

[111] J. Delaey, P. Dubruel, S. Van Vlierberghe, *Adv. Funct. Mater.* **2020**, *30*, 1909047.

[112] A. Amirkiai, M. Abrisham, M. Panahi-Sarmad, X. Xiao, A. Alimardani, M. Sadri, *Mater. Today Commun.* **2021**, *28*, 102658.

[113] P. Fei, K. A. Cavicchi, *ACS Appl. Mater. Interfaces* **2010**, *2*, 2797.

[114] M. N. I. Shiblee, K. Ahmed, M. Kawakami, H. Furukawa, *Adv. Mater. Technol.* **2019**, *4*, 1900071.

[115] Z. Zhao, C. Li, Z. Dong, Y. Yang, L. Zhang, S. Zhuo, X. Zhou, Y. Xu, L. Jiang, M. Liu, *Adv. Funct. Mater.* **2019**, *29*, 1807858.

[116] X. Shen, F. Wang, Z. Mao, H. Xu, B. Wang, X. Sui, X. Feng, *Chem. Eng. J.* **2021**, *416*, 129181.

[117] C. Bilici, V. Can, U. Nöchel, M. Behl, A. Lendlein, O. Okay, *Macromolecules* **2016**, *49*, 7442.

[118] K. Peng, H. Yu, H. Yang, X. Hao, A. Yasin, X. Zhang, *Soft Matter* **2017**, *13*, 2135.

[119] K. Liu, Y. Zhang, H. Cao, H. Liu, Y. Geng, W. Yuan, J. Zhou, Z. L. Wu, G. Shan, Y. Bao, Q. Zhao, T. Xie, P. Pan, *Adv. Mater.* **2020**, *32*, 2001693.

[120] F. Wang, X. Yong, J. Deng, Y. Wu, *RSC Advances* **2018**, *8*, 16773.

[121] H. Zhang, D. Han, Q. Yan, D. Fortin, H. Xia, Y. Zhao, *J. Mater. Chem. A* **2014**, *2*, 13373.

[122] H. Jing, L. He, J. Feng, H. Fu, S. Guan, P. Guo, *Soft Matter* **2019**, *15*, 5264.

[123] X. Chang, Y. Geng, H. Cao, J. Zhou, Y. Tian, G. Shan, Y. Bao, Z. L. Wu, P. Pan, *Macromol. Rapid Commun.* **2018**, *39*, 1700806.

[124] R. Pelrine, R. Kornbluh, Q. Pei, J. Joseph, *Science* **2000**, *287*, 836.

[125] Y. Qiu, E. Zhang, R. Plamthottam, Q. Pei, *Acc. Chem. Res.* **2019**, *52*, 316.

[126] M. M. Seyed, W. H. Ian, *Adv. Mater.* **2017**, *30*, 1704407.

[127] F. Carpi, I. Anderson, S. Bauer, G. Frediani, G. Gallone, M. Gei, C. Graaf, C. Jean-Mistral, W. Kaal, G. Kofod, M. Kollosche, R. Kornbluh, B. Lassen, M. Matysek, S. Michel, S. Nowak, B. O'Brien, Q. Pei, R. Pelrine, B. Rechenbach, S. Rosset, H. Shea, *Smart Materials and Structures* **2015**, *24*, 105025.

[128] Z. Yu, W. Yuan, P. Brochu, B. Chen, Z. Liu, Q. Pei, *Appl. Phys. Lett.* **2009**, *95*, 192904.

[129] X. Niu, X. Yang, P. Brochu, H. Stoyanov, S. Yun, Z. Yu, Q. Pei, *Adv. Mater.* **2012**, *24*, 6513.

[130] Z. Peng, Y. Qiu, Y. Shi, Z. Zhang, A. Alwen, H. Yin, R. Plamthottam, Z. Ren, Q. Pei, *Proc. SPIE* **2019**, *10966*, 109662C.

[131] N. Besse, S. Rosset, J. J. Zarate, H. Shea, *Adv. Mater. Technol.* **2017**, *2*, 1700102.

[132] X. Yu, M. Yuan, W. Wenxin, Z. Elric, L. Jinsong, P. Qibing, *Adv. Funct. Mater.* **2018**, *0*, 1802430.

[133] J. Meng, Y. Qiu, C. Hou, Q. Zhang, Y. Li, H. Wang, *Sens. Actuators A* **2021**, *330*, 112889.

[134] Y. J. Ke, J. W. Chen, C. J. Lin, S. C. Wang, Y. Zhou, J. Yin, P. S. Lee, Y. Long, *Adv. Energy Mater.* **2019**, *9*, 1902066.

[135] Y. Ke, C. Zhou, Y. Zhou, S. Wang, S. H. Chan, Y. Long, *Adv. Funct. Mater.* **2018**, *28*, 1800113.

[136] J. Dean, *Lange's Handbook of Chemistry*, McGRAW-Hill, Inc., 1999.

[137] J.-G. Liu, M. Ueda, *J. Mater. Chem.* **2009**, *19*, 8907.

[138] Y. Xie, F. Guan, Z. Li, Y. Meng, J. Cheng, L. Li, Q. Pei, *Macromol. Rapid Commun.* **2020**, *41*, 2000290.

[139] R. Pritchard, *Polym. Eng. Sci.* **1964**, *4*, 66.

[140] C. R. López-Barrón, A. H. Tsou, J. M. Younker, A. I. Norman, J. J. Schaefer, J. R. Hagadorn, J. A. Throckmorton, *Macromolecules* **2018**, *51*, 872.

[141] R. M. Michell, A. J. Müller, *Prog. Polym. Sci.* **2016**, *54-55*, 183.

[142] Y. Suzuki, H. Duran, M. Steinhart, H.-J. Butt, G. Floudas, *Soft Matter* **2013**, *9*, 2621.

[143] H. Wang, J. K. Keum, A. Hiltner, E. Baer, B. Freeman, A. Rozanski, A. Galeski, *Science* **2009**, *323*, 757.

[144] Y. Lin, E. Bilotti, C. W. M. Bastiaansen, T. Peijs, *Polym Eng Sci.* **2020**, *60*, 2351.

[145] X.-H. Li, C. Liu, S.-P. Feng, N. X. Fang, *Joule* **2019**, *3*, 290.

[146] J. Mandal, M. Jia, A. Overvig, Y. Fu, E. Che, N. Yu, Y. Yang, *Joule* **2019**, 1.

[147] H. Moosmüller, R. K. Chakrabarty, W. P. Arnott, *J. Quant. Spectrosc. Radiat. Transfer* **2009**, *110*, 844.

[148] X. Fan, W. Zheng, D. J. Singh, *Light: Sci. Appl.* **2014**, *3*, 179.

[149] D. Filingeri, H. Zhang, E. A. Arens, *J. Neurophysiol.* **2017**, *117*, 1797.

[150] Y. Liu, J. C. Fan, R. Plamthottam, M. Gao, Z. H. Peng, Y. Meng, M. F. He, H. X. Wu, Y. F. Wang, T. X. Liu, C. Zhang, Q. B. Pei, *Chem. Mater.* **2021**, *33*, 7232.

[151] S. Deng, L. Huang, J. Wu, P. Pan, Q. Zhao, T. Xie, *Adv. Mater.* **2021**, *33*, 2008119.

[152] D. K. Hohl, C. Weder, *Adv. Opt. Mater.* **2019**, *7*, 1900230.

[153] C. Bandl, W. Kern, S. Schlögl, *Int. J. Adhes. Adhes.* **2020**, *99*, 102585.

[154] W. Li, X. Liu, Z. Deng, Y. Chen, Q. Yu, W. Tang, T. L. Sun, Y. S. Zhang, K. Yue, *Adv. Mater.* **2019**, *31*, 1904732.

[155] Y. Zhao, Y. Wu, L. Wang, M. Zhang, X. Chen, M. Liu, J. Fan, J. Liu, F. Zhou, Z. Wang, *Nat. Commun.* **2017**, *8*, 2218.

[156] P. Rao, T. L. Sun, L. Chen, R. Takahashi, G. Shinohara, H. Guo, D. R. King, T. Kurokawa, J. P. Gong, *Adv. Mater.* **2018**, *30*, 1801884.

[157] X. Chen, H. Yuk, J. Wu, C. S. Nabzdyk, X. Zhao, *Proc. Natl. Acad. Sci. U. S. A.* **2020**, *117*, 15497.

[158] J.-W. Seo, H. Kim, K. Kim, S. Q. Choi, H. J. Lee, *Adv. Funct. Mater.* **2018**, *28*, 1800802.

[159] H. Lee, D.-S. Um, Y. Lee, S. Lim, H.-j. Kim, H. Ko, *Adv. Mater.* **2016**, *28*, 7457.

[160] Y. Huang, N. Zheng, Z. Cheng, Y. Chen, B. Lu, T. Xie, X. Feng, *ACS Appl. Mater. Interfaces* **2016**, *8*, 35628.

[161] C.-M. Chen, C.-L. Chiang, C.-L. Lai, T. Xie, S. Yang, *Adv. Funct. Mater.* **2013**, *23*, 3813.

[162] A. N. Gent, G. R. Hamed, *Polym Eng Sci.* **1977**, *17*, 462.

[163] J. Kim, D. W. Kim, S. Baik, G. W. Hwang, T.-i. Kim, C. Pang, *Adv. Mater. Technol.* **2019**, *4*, 1900316.

[164] H. Yuk, T. Zhang, S. Lin, G. A. Parada, X. Zhao, *Nat. Mater.* **2016**, *15*, 190.

[165] Y. Qiu, S. Ma, Q. Pei, J. D. Holbery, *Adv. Intell. Syst.* **2019**, *1*, 1900054.

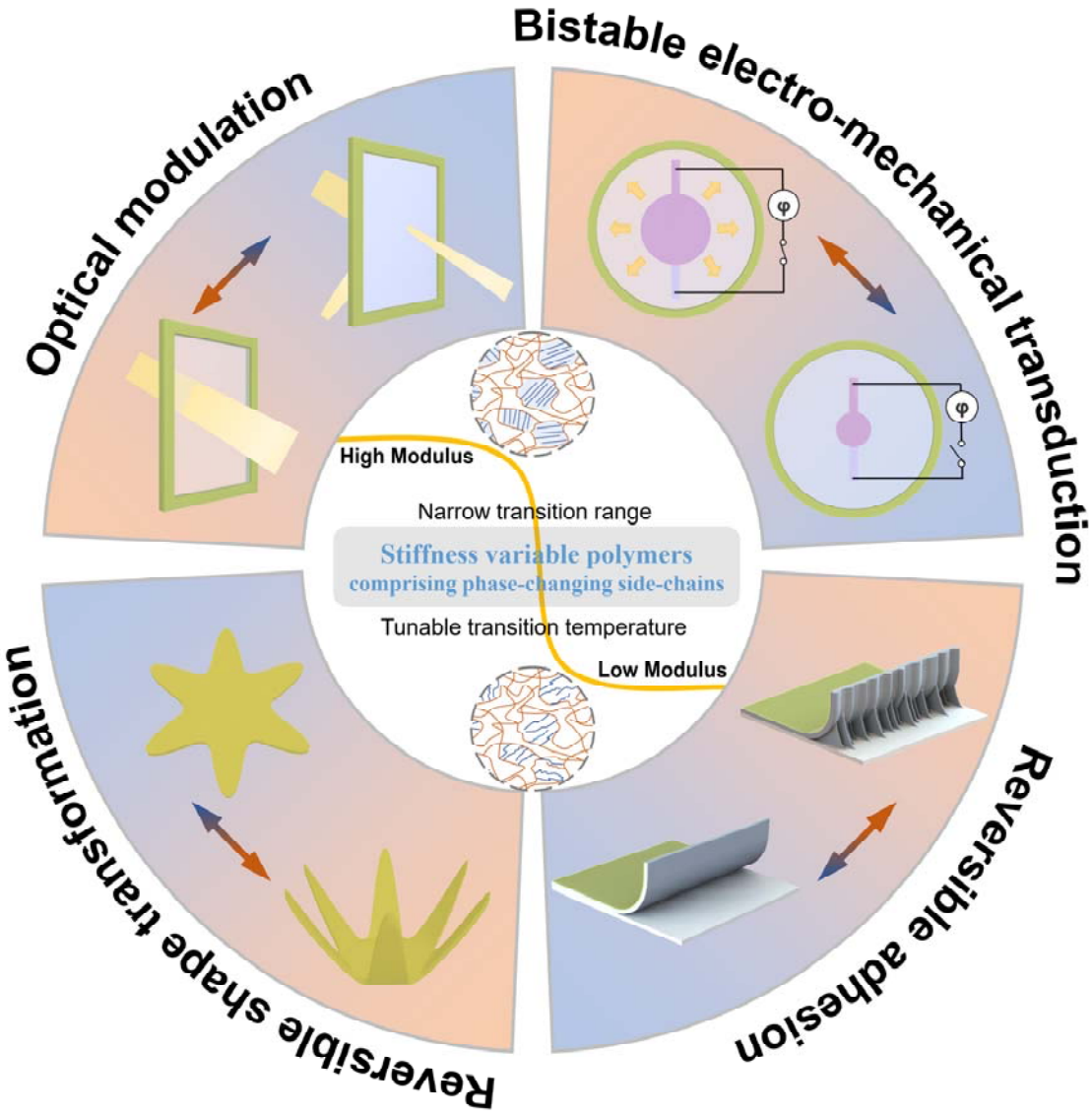

Figure 1. An overview of the mechanism, features, and applications of stiffness variable polymers comprising phase-changing side-chains.

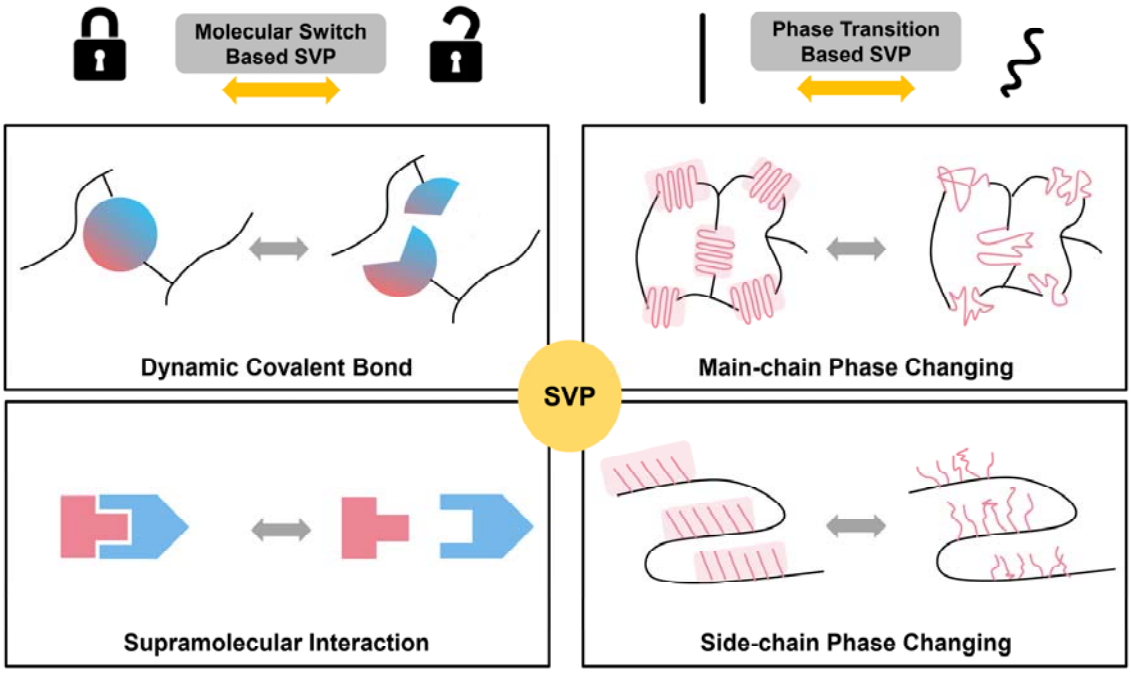

Figure 2. Classification of stiffness variable polymers based on the triggering mechanism and molecular structure.

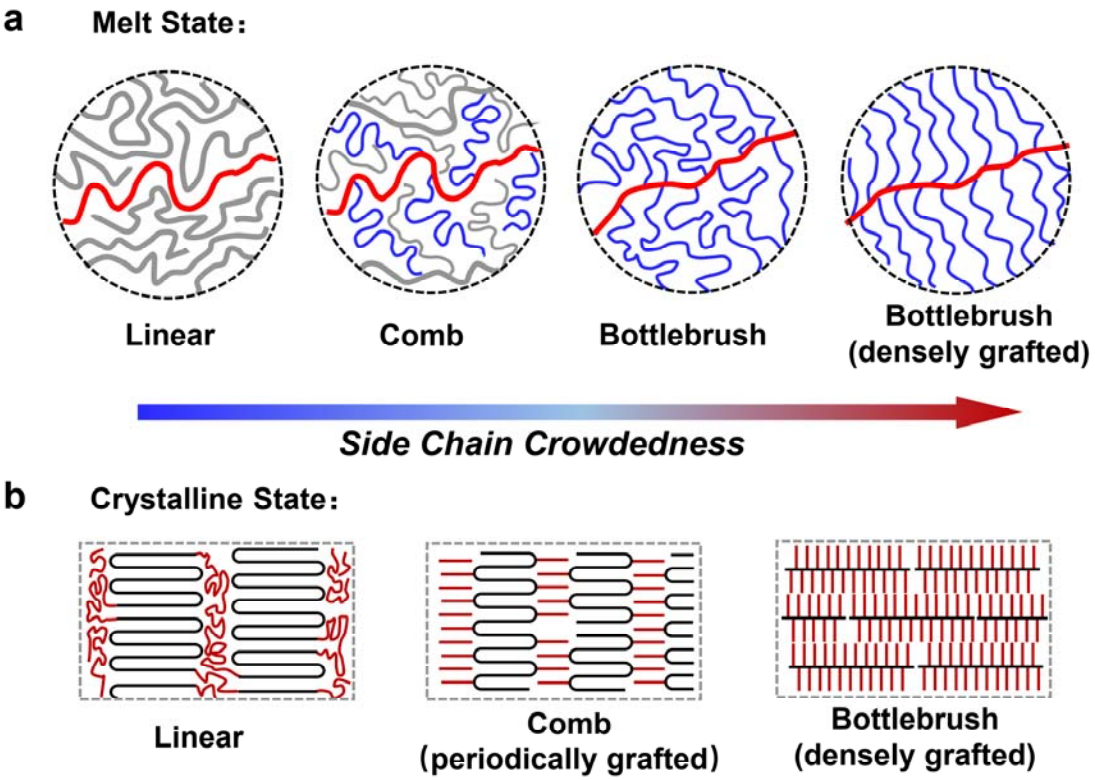

Figure 3. Melt state a) and Crystalline state b) as the side chain crowdedness increases, illustrating the mechanism of s-SVP's large modulus change.

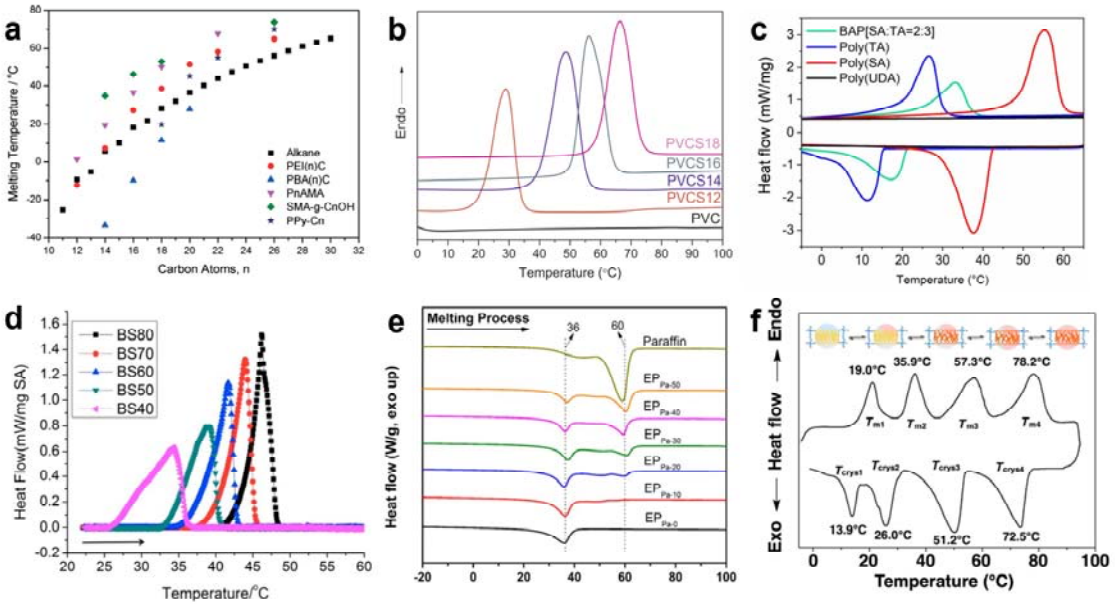

Figure 4. Transition temperature of s-SVP and the corresponding copolymers and composites. a) Melting temperature vs. carbon atoms of the side-chain in various s-SVP. Reproduced with permission.[79] Copyright 2014, Royal Society of Chemistry. b) Differential scanning calorimetry (DSC) of alkylated poly(vinyl chloride) with different side-chain carbon atom numbers. Reproduced with permission[77] Copyright 2018, Elsevier. c) DSC of stearyl acrylate, tetradecyl acrylate, and its copolymers.[50] Copyright 2021, The Authors, Cellpress. d) DSC of stearyl acrylate - urethane diacrylate copolymers of different ratios.[52] Copyright 2016, The Authors, American Chemical Society. e) DSC of allyl-based epoxy resin - paraffin composites of different ratios. Reproduced with permission.[99] Copyright 2018, American Chemical Society. f) DSC of composites comprising poly(stearyl methacrylate) and n-alkanes series with different alkyl chain lengths. Reproduced with permission.[100] Copyright 2020, Science Publishing Group.

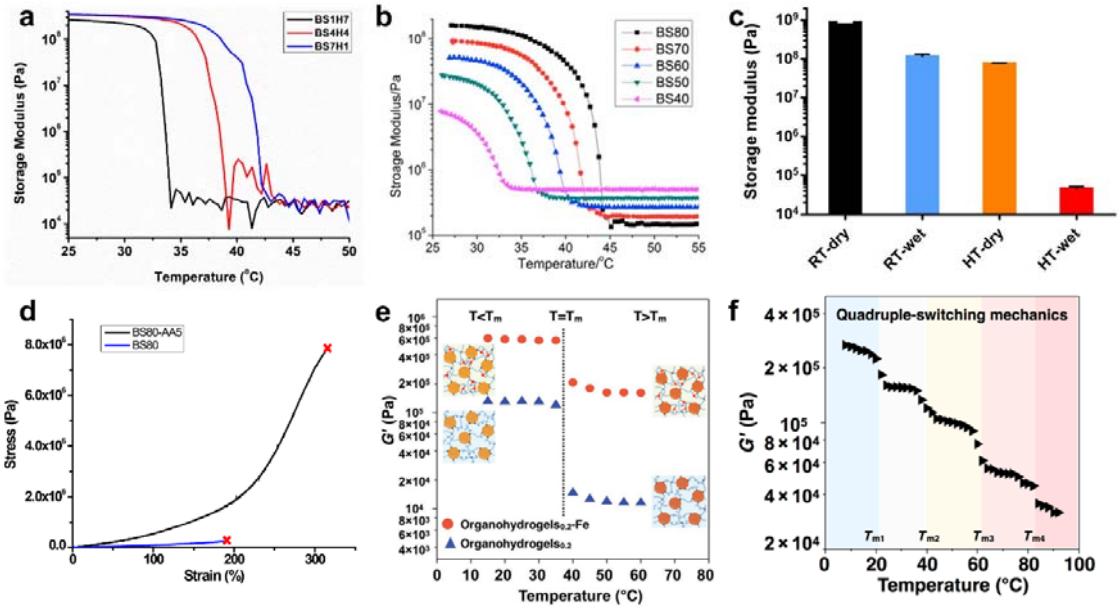

Figure 5. Mechanical property of s-SVP copolymers and composites.
a) Storage modulus versus temperature curve of hexadecyl acrylate-stearyl acrylate copolymers of different ratios.[101] Copyright 2020, The Authors, American Chemical Society. b) Storage modulus versus temperature curve of stearyl acrylate - urethane diacrylate copolymers of different ratios.[52] Copyright 2016, The Authors, American Chemical Society. c) The storage modulus measurement of s-SVP reinforced by bacterial cellulose nanofibers at different states.[101] Copyright 2020, The Authors, American Chemical Society. d) Tensile stress-strain curve of s-SVP and s-SVP -acrylic acid composite above the transition temperature.[104] Copyright 2018, The Authors, American Chemical Society. e) Storage modulus versus temperature curve s-SVP corporated with tridentate Fe(III) - carboxylate reversible group under association/dissociation stimuli. Reproduced with permission.[105] Copyright 2018, Wiley-VCH. f) Storage modulus versus temperature curve of composites comprising poly(stearyl methacrylate) and n-alkanes series with different alkyl chain lengths. Reproduced with permission.[100] Copyright 2020, published by Science Publishing Group.

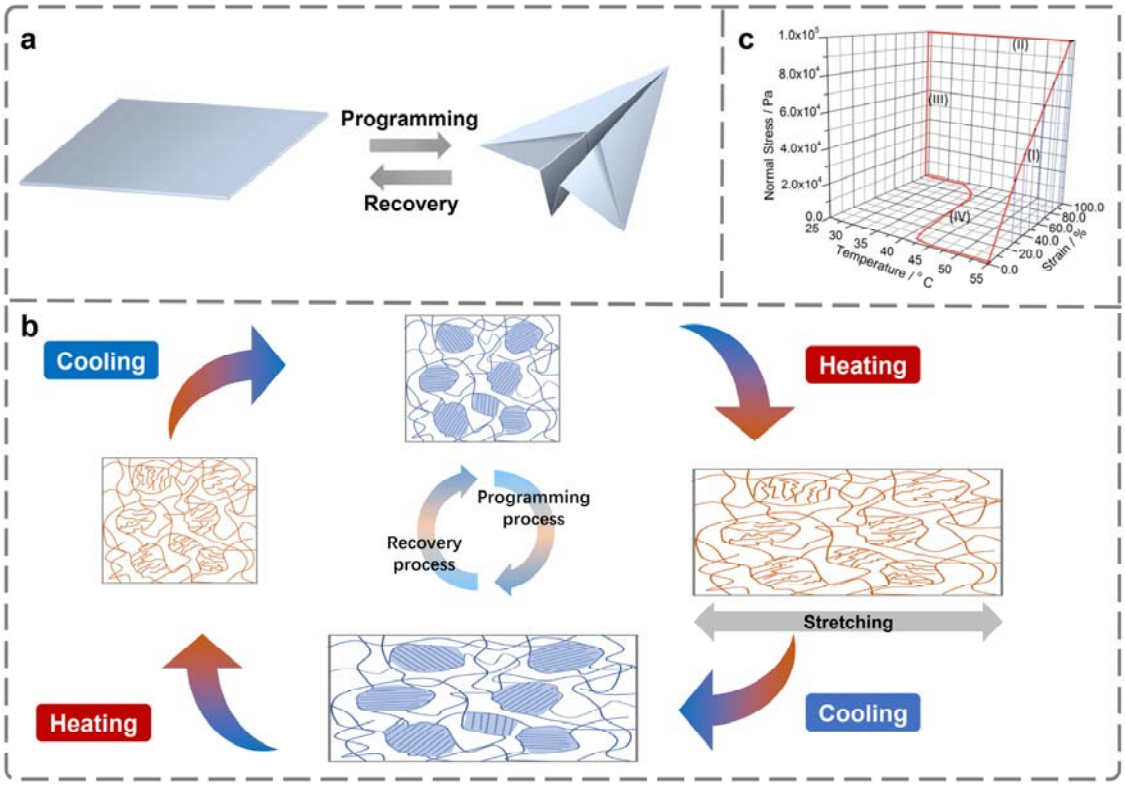

Figure 6. Mechanism and representative reversible shape transformation process of s-SVP. a) Programming and recovery process of shape memory effect. b) Working mechanism and process of s-SVP based shape memory performance. c) 3D stress-strain-temperature of the shape memory cycle.[52] Copyright 2016, The Authors, published by American Chemical Society.

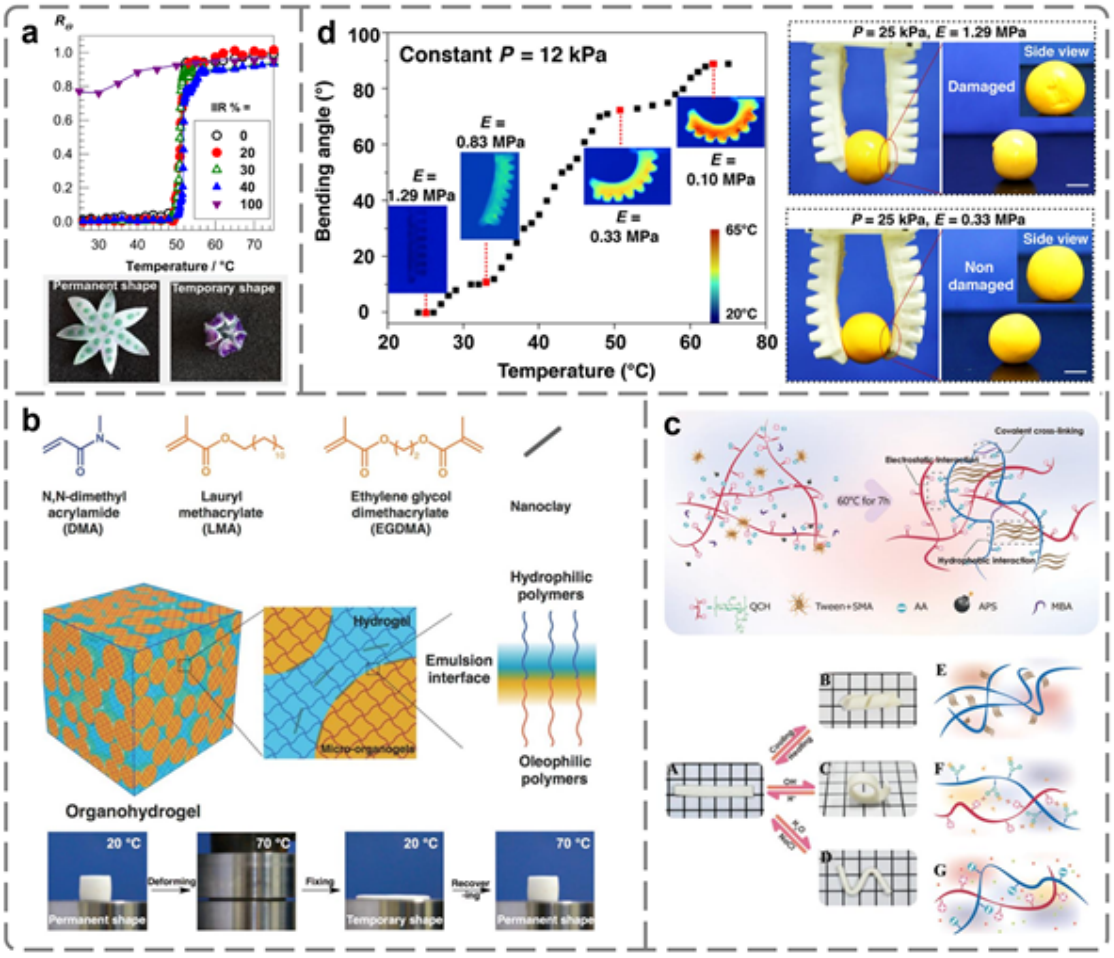

Figure 7. Reversible shape transformation performance of s-SVP.
a) Shape recovery efficiency and shape recovery process of interpenetrating polymer network based on poly(n-octadecyl acrylate) butyl rubber. Reproduced with permission.[98] Copyright 2021, American Chemical Society. b) High strain capacity and excellent shape memory behavior of the organohydrogel prepared by in-situ polymerization of an emulsion system that contained hydrophilic N, N-dimethyl acrylamide, and hydrophobic lauryl methacrylate monomers. Reproduced with permission.[102] Copyright 2017, Wiley-VCH. c) Organohydrogel with multiple shape memory effect responsive to different stimuli is fabricated by copolymerizing stearyl methacrylate, acrylic acid, and quaternary chitosan. Reproduced with permission.[122] Copyright 2019, Royal Society of Chemistry. d) Programmable organohydrogels with varying applicable mechanical properties through stepwise manipulation of the noneutectic phase transitions, and the application in stiffness adaptive soft robotic gripper. Reproduced with permission.[100] Copyright 2020, Science Publishing Group.

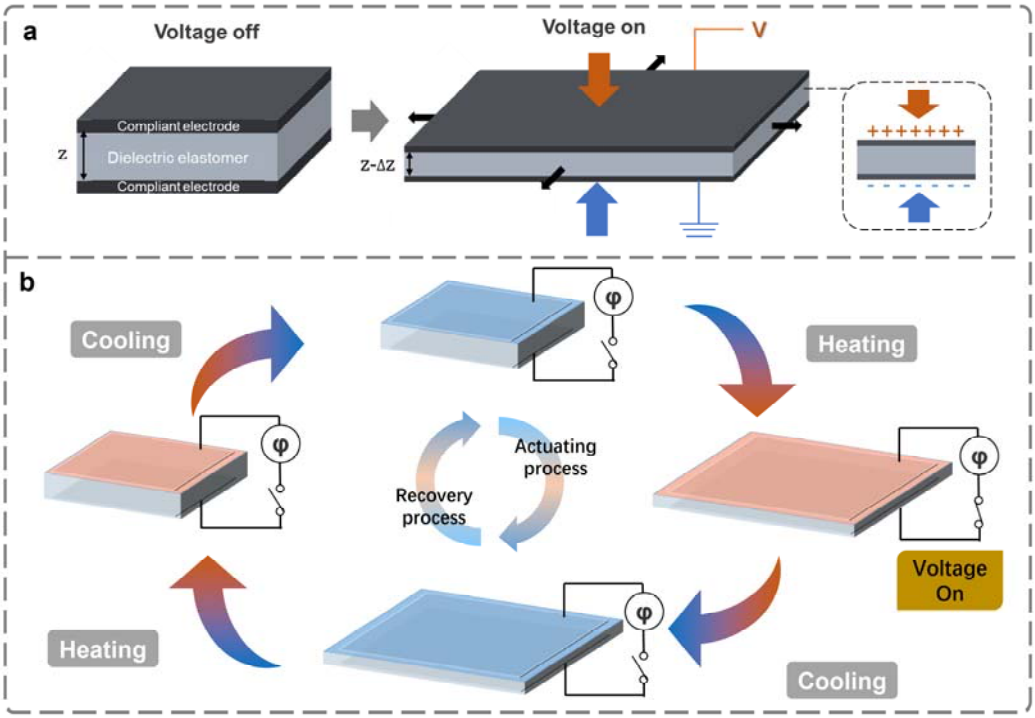

Figure 8. Mechanism and representative bistable electromechanical transduction process of s-SVP based BSEP.
a) Operating principle of dielectric elastomer actuator. b) Working mechanism and process of BSEP based bistable dielectric elastomer actuator.

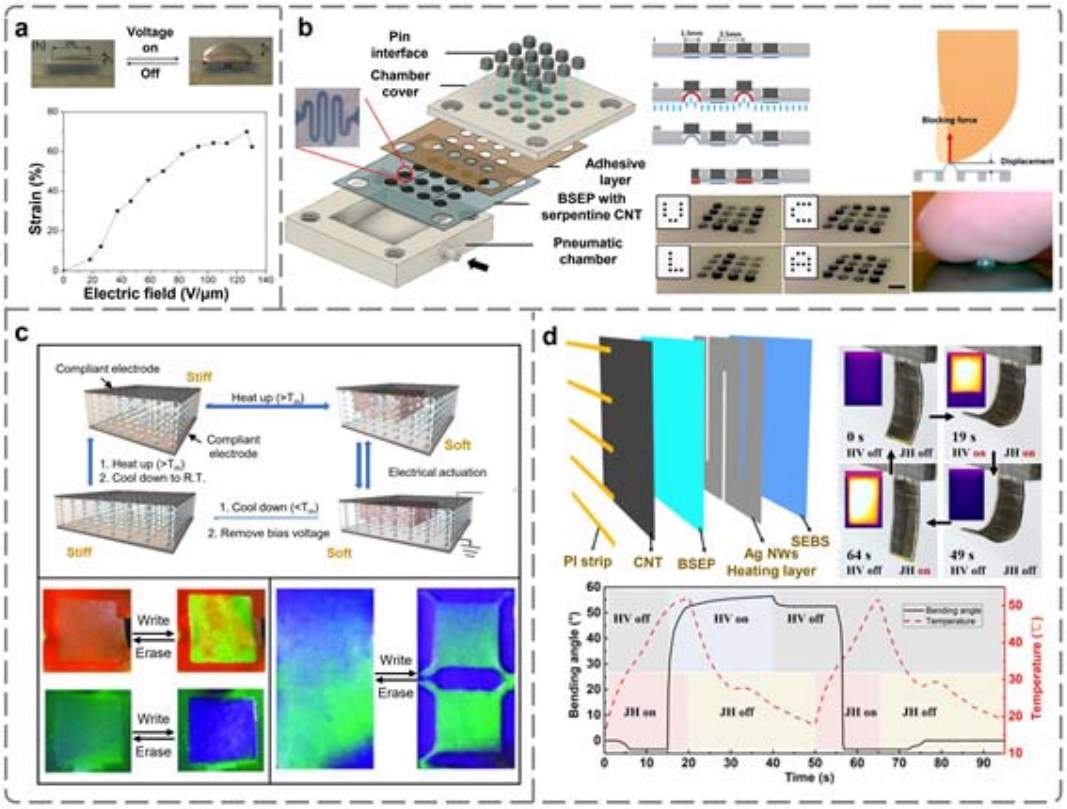

Figure 9. Application of s-SVP based dielectric elastomer actuator exhibiting bistable electromechanical transduction.
a) Actuation performance of BSEP based dielectric elastomer actuator photopolymerized from s-SVP stearyl acrylate and crosslinker long-chain urethane diacrylate.[52] Copyright 2016, The Authors, American Chemical Society. b) Working principle and demonstration of refreshable tactile display based on a BSEP and stretchable serpentine joule heating electrode.[104] Copyright 2018, The Authors, American Chemical Society. c) Modulus and reflectivity of rewritable paper consisting of ferroferric oxide-carbon (Fe3O4@C) core-shell nanoparticles - based photonic crystal embedded in BSEP. Reproduced with permission.[132] Copyright 2018, The Authors, Wiley-VCH. d) The bistable dielectric elastomer actuators developed by bilayer structure made from BSEP and passive layer. Reproduced with permission.[133] Copyright 2021, Elsevier.

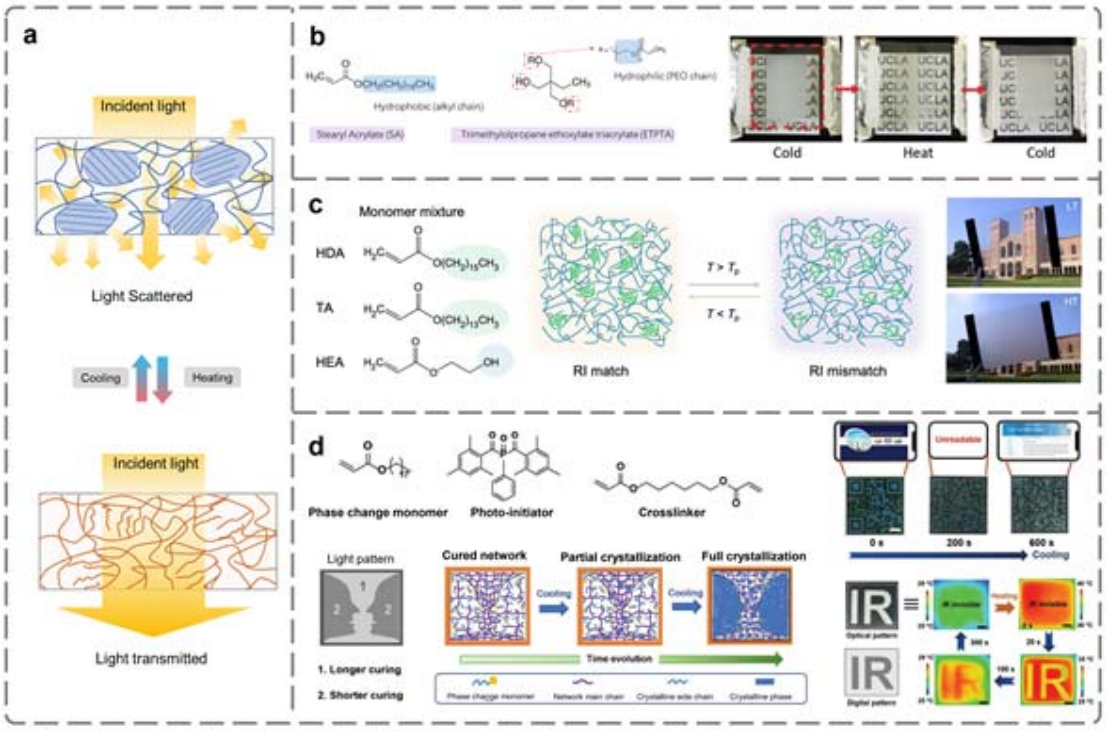

Figure 10. S-SVP's mechanism and applications in optical modulation.
a) Mechanism of transmittance modulation based on the tunable scattering behaviors of s-SVP. b) A polymer film of the poly(stearyl acrylate) crosslinked with a poly(ethylene oxide) oligomer is synthesized, which demonstrates tunable opacity to regulate solar irradiation and privacy protection.[138] Copyright 2020, The Authors, Wiley-VCH. c) A broadband optical modulator with a transition temperature at 28−32 °C is built by crosslinking a hydrophilic poly(hydroxyethyl acrylate with a hydrophobic phase-changing poly(hexadecyl acrylate-tetradecyl acrylate) (HDA-TA). The film stays transparent at room temperature, allowing sunlight to pass through, and turn opaque at high temperature to block solar radiation.[150] Copyright 2021, The Authors, American Chemical Society. d) A digitally light-cured poly (stearyl acrylate) with different cross-linking degrees is designed for programming temporal optical and thermal information. Reproduced with permission. [151] Copyright 2021, Wiley-VCH.

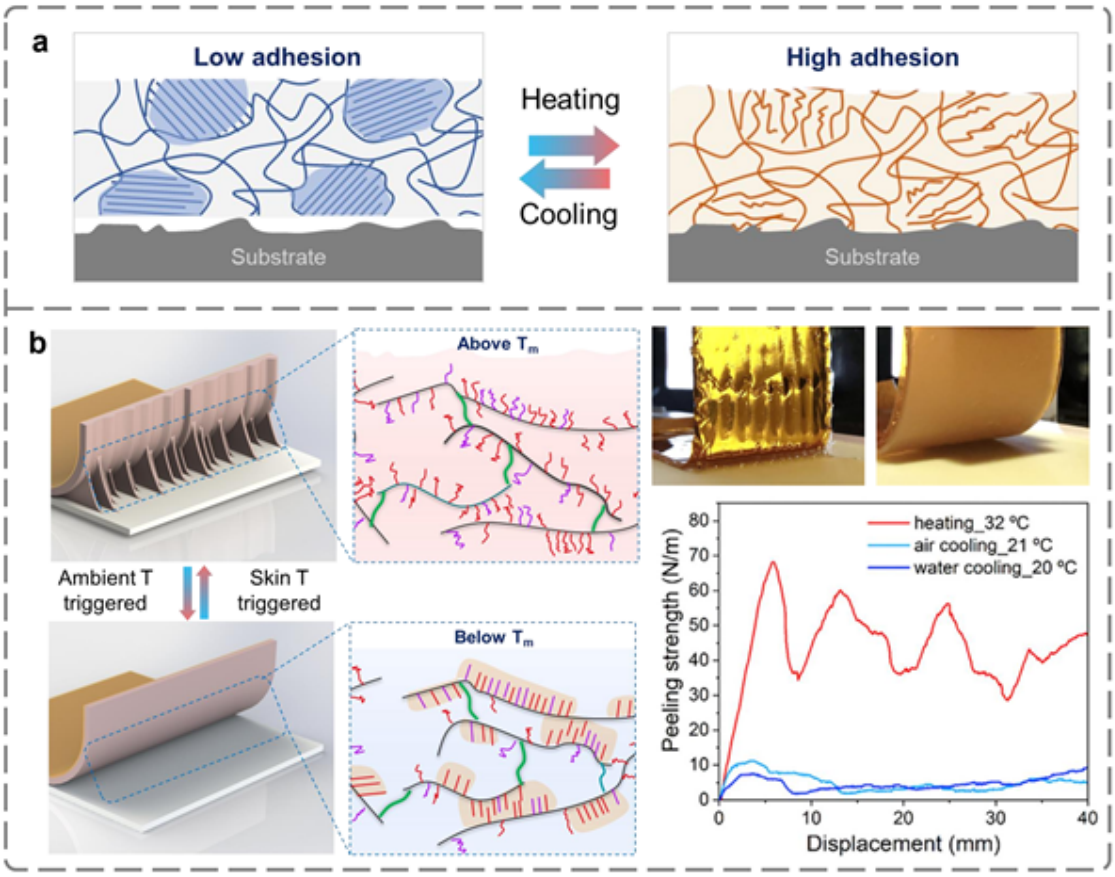

Figure 11. S-SVP's s mechanism and applications in reversible adhesion.
a) Working mechanism of s-SVP's reversible adhesion tuning behavior. b) Bistable adhesive polymer with skin temperature-triggered conformal adhesion and room temperature-triggered easy detaching is prepared by incorporating stearyl acrylate and tetradecyl acrylate into a chemically crosslinked elastomer.[50] Copyright 2021, The Authors, Cellpress.

Table 1. Representative of s-SVPs and their thermal/mechanical performances.

S-SVP material types (abbreviation)	Backbone group	Alkyl chain length	Additives	Transition temperature [°C]	Transition temperature span [°C]	Modulus variation [MPa]	Ref.
PnA	polyacrylate	18	N/A	48.5	~5	-	[74]
PnMA	polymethacrylate	18	N/A	37.0	~5	-	[75]
n-PEI	poly(ethyleneimine)	18	N/A	36.8	~8	-	[91]
n-PEI	poly(ethyleneimine)	20	N/A	51.9	~10	-	[90]
n-EP	epoxy resin	18	N/A	36	~12	-	[76]
n-PVA	poly(vinyl alcohol)	18	N/A	51.1	~13	-	[78]
n-PVC	S-alkylated-poly(vinyl chloride)	12-18	N/A	36.0-66.3	~15	-	[77]
PPy	poly(pyrrole)	20-26	N/A	19.8-70.0	~18-12	-	[79]
PBA	poly(p-benzamide)	18	N/A	11.6	~22	-	[91]
n-PANi	Polyanilines	18	N/A	20	~25	-	[92]
PnMA	polymethacrylate	18	polystyrene	18	~6	-	[57]
PnA	polyacrylate	14,18	UDA elastomer	25-48	~6	0.03-30.8	[50]
PnA	polyacrylate	18	Butyl rubber	52.0	~9	9-34	[98]
PnMA	polymethacrylate	18	PAAm-co-PAA hydrogel, n-alkenes	19.3，35.0，57.3	~7	0.10-1.29	[100]
PnA	polyacrylate	18	PAA hydrogel	51.0	~5	0.008-9	[117]
PnMA	polymethacrylate	18	Fe(III)–carboxylate based hydrogel	37.4	~6	0.055-57	[105]
PnA	polyacrylate	18	UDA, acrylic acid	43	~7	0.1-300	[104]
PnA	polyacrylate	16,18	UDA,bacterial cellulose	37	~6	0.04-1000	[101]

Polymers comprising side chains undergoing reversible crystallization and melting in narrow temperature span have been synthesized for stiffness control. A modulus change of more than 1000 fold can be achieved. Larger stiffness changes could be obtained. The phase-changing can additionally be exploited for reversible adhesions, bistable actuation, and opacity modulation. Important applications will be discussed.

Meng Gao, Yuan Meng,* Claire Shen, and Qibing Pei*

Stiffness variable polymers comprising phase-changing side-chains: material syntheses and application explorations